Supplementary materials for Biophysical factors and management practices are key to shaping forest resilience

Authors: Yu Yan[1,2 #], Xingyu Feng[1,2 #], Zhiyong Liu[1,2*], Zizhao Wang[3], Zeqin Huang[1,2], Yajun Wang[4], Xin Lan[5], Juan Chen [6], Kairong Lin[1,2], Xiaohong Chen[1,2], Chunyu Dong[1,2], Xiaogang He[7], Giovanni Forzieri[8]

Affiliations:

[1]Center for Water Resources and Environment, School of Civil Engineering, Sun Yat-sen University, Guangzhou 510275, China

[2]Southern Marine Science and Engineering Guangdong Laboratory (Zhuhai), Zhuhai 519082, China

[3]School of Life Sciences, Peking University, Beijing 100871, China

[4]Institute of Estuarine and Coastal Research, School of Ocean Engineering and Technology, Sun Yat-sen University, Guangzhou 510275, China

[5]College of Agricultural Science and Engineering, Hohai University, Nanjing 210098, China

[6]Key Laboratory of Eco-environments in Three Gorges Reservoir Region of Ministry of Education, School of Life Sciences, Southwest University, Chongqing 400715, China

[7]Department of Civil and Environmental Engineering, National University of Singapore, Singapore 117576, Singapore

[8]Department of Civil and Environmental Engineering, University of Florence, Florence, Italy

*Corresponding author: Zhiyong Liu (liuzhiy25@mail.sysu.edu.cn)

[#]Contribution equals in this work: Yu Yan and Xingyu Feng

Supplementary Note1~Note9:

Supplementary Note 1: The impacts of forest management on ecological resilience and functions.

Our analysis indicates that natural forests without management (NF WOM) have 13% higher resilience than natural forests with management (NF WM) (Supplementary Fig. 3). This suggests that forest management may reduce the resilience of natural forests by about 13%. It should be noted that this 13% difference represents an average effect globally. Under specific conditions, such as in dry climates or areas with deep root systems, the reduction in resilience caused by management can become much larger, reaching two to three times the average loss. This pattern aligns with findings from previous studies on forest ecosystem functions. For example, unmanaged forests are reported to store two to four times more carbon than managed forests[1–4]. In some regions, this disparity can exceed tenfold, i.e. NF WOM may store more than ten times as much carbon as NF WM. Moreover, management practices negatively impact other ecosystem functions, including water regulation[5–7] and soil fertility[8,9]. These impacts become even more pronounced under intensive management, such as in Plantations. Compared to NF WOM, the deficits of Plantations in soil fertility, carbon storage, and water regulation are even larger than those observed between NF WM and NF WOM[10]. Their resilience follows similar patterns: Plantations exhibit about 20% lower resilience than NF WOM, which is a greater loss than the loss between NF WM and NF WOM (Supplementary Fig. 3). These observations confirm that ecosystem resilience is tightly linked to broader ecological functions. Lower resilience reduces the ability of forests to buffer disturbances, ultimately weakening forest services and ecological stability[11].

Supplementary Note 2: Influence of biophysical factors on resilience differences among forest management types.

We further develop four XGBT models to explore the relationships between resilience differences and environmental factors (Supplementary Fig. 17). Specifically, the models analyze resilience differences ($\Delta\lambda$AR1-LAI, target) between NF and Plantations, NF WOM and F WM, NF WOM and NF WM, and NF WOM and Plantations. The environmental factors (i.e., predictors) include annual temperature (Temp), dryness index (P/PET), root depth (RD), above-ground biomass (AGB), below-ground biomass (BGB), clay fraction (Clay), sand fraction (Sand), and cation exchange capacity (CEC). The overall performance of these models, as measured by the KGE (Kling-Gupta Efficiency) on testing samples, ranged from 0.6 to 0.7 (Supplementary Fig. 17), indicating good performance.

The results highlight temperature as the most important factor in predicting the resilience differences between NF and Plantations, and between NF WOM and Plantations (Supplementary Fig. 17a, d). Higher average temperature may exacerbate the resilience differences. In regions with high average temperatures (e.g., tropical regions), Plantations are often dominated by monoculture cash crops, such as oil palm, which lack the structural and biological complexity compared to natural forests[12,13]. Structural complexity is important for forest resilience. A complex canopy provides microclimate cooling effects[14]. It helps maintain higher humidity and lower temperatures under the canopy, which reduces heat and drought stress of disturbances and supports to absorb the disturbances and maintain equilibrium. In addition, complex canopy layers offer functional redundancy. When the upper canopy is damaged by disturbance, the lower canopy can grow rapidly and help maintain stable biomass[15,16]. Therefore, in regions with high average temperatures, the structural complexity of Plantations is lower than that of natural forests, which may contribute to the resilience differences.

The root depth is the most important factor influencing resilience differences between NF WM and NF WOM, or F WM and NF WOM. Results reveal that regions with larger root depth may have larger resilience gaps (Supplementary Fig. 17b, c). Forests with deep root systems can access groundwater, which helps buffer against drought and water stress from disturbances[17]. However, management practices can disrupt this access through irrigation[18], making forests, such as NF WM and F WM, more sensitive to drought or water variability, thereby significantly reducing resilience. This contrast is particularly evident in mountainous regions, where steep terrain, shallow soils, and strong environmental heterogeneity promote the development of complex and deep root systems. The complex and deep root system in NF WOM enhances soil stability, water retention, and biodiversity, together supporting higher resilience. In contrast, management in these regions (e.g., NF WM) tends to simplify root systems, degrade soil quality, and reduce biodiversity, leading to greater resilience loss[19]. Moreover, in mountainous regions, vegetation canopies are often well developed while root zones remain relatively shallow, creating a canopy–root zone imbalance (i.e., structure overshoot[20]). This structural mismatch reduces the capacity of the belowground system to support the complex aboveground vegetation, thereby lowering the resilience of forests when root systems are disturbed by management.

Overall, these results suggest that resilience differences among managed forests are strongly shaped by interactions between management practices and biophysical conditions, highlighting the need for adaptive strategies tailored to local climates and ecosystems (Fig. 4 and Supplementary Fig. 17).

Supplementary Note 3: Sensitivity tests in paired grid settings.

Effects of disturbance and ecological background in paired grids: Differences in disturbance regimes and ecological backgrounds between paired forest types may also influence the resilience comparisons. For example, NF WM may experience more intensive logging, which could lead to lower resilience compared to NF WOM. To address this uncertainty, we use the GFCC (Global Forest Cover Change) dataset to extract the disturbance (e.g., deforestation or afforestation intensity), which provides 30 m forest cover data at five-year intervals from 2000 to 2015. We then calculate the change in forest cover ($FCC = FC_{2015} - FC_{2000}$) over this period. For ecological background, we use 300 m aboveground biomass data for 2010 from the NASA/ORNL dataset. Both FCC and biomass are resampled to 1000 m to match the resolution of resilience metrics. In grids, we initially restrict the average differences in elevation and forest age to within 500 m and 10 years, respectively. We further quantify the differences in forest cover change and biomass between two forest management types, e.g., $\Delta FCC_{(PF, NF)} = |FCC_{PF} - FCC_{NF}|$ or $\Delta AGB_{(PF, NF)} = |AGB_{PF} - AGB_{NF}|$. We constrain paired grids by also limiting differences in forest cover change and biomass. For example, we retain only those paired grids where the FCC difference between PF and NF is within 10%, 5%, or 3%, or where the AGB difference is within 10 Mg/ha or 5 Mg/ha.

Under different thresholds of forest cover change and aboveground biomass differences, the patterns of resilience differences remain consistent across vegetation indices (Supplementary Fig. 21). Specifically, unmanaged natural forests (NF WOM) consistently show higher resilience than Plantations, while NF WM generally exhibits lower resilience than NF WOM. The largest resilience difference is observed between NF WOM and Plantations, followed by NF WOM versus F WM, and NF WOM versus NF WM. These results further support the conclusion that resilience differences are primarily driven by management practices rather than by disturbance regimes or ecological background.

Supplementary Note 4: Sensitivity tests about the influence of data preprocessing on resilience estimation

Effect of three vegetation data treatments on resilience estimation: To ensure reliable resilience estimation, we evaluate the influence of data pre-processing on vegetation time series. Vegetation datasets contain missing values caused by snow and cloud cover, which may impact the resilience estimation. We mitigate the effects of clouds and snow through quality control (QC) flags and retain only the high-quality data in the vegetation products. All vegetation products are resampled to 1 km resolution. We further test three data processing approaches (Supplementary Figs. 22-25):

(1) Monthly MVC composites (method in the main text): combining MODIS Terra and Aqua data and selecting the maximum value within each month to minimize cloud and snow contamination,

(2) Terra-only time series: using vegetation data from MODIS Terra at its original temporal resolution.

(3) Terra-only growing-season time series: using Terra data restricted to the growing season, defined by a temperature threshold of $T > 5$ °C[21].

Resilience indicators (λAR1, λVar, AR1) are estimated under these three settings. Resilience differences among forest management types are further quantified using a moving-window approach. These three data processing approaches are selected based on previous studies[11,22], to test the sensitivity of resilience estimation to temporal aggregation, sensor selection, and missing values. It should be noted that these three approaches are not equally applicable to all vegetation indices. For GPP_PML, which is available as a single product rather than separate Terra and Aqua streams, we slightly modify the processing strategy. Specifically, we apply (1) MVC to generate monthly maximum values, (2) retain the original 8-day resolution series, and (3) use the original 8-day resolution data but restricted to the growing season. In this way, the three settings remain comparable to those applied to other vegetation indices.

Overall, the three preprocessing approaches yield highly consistent results (Supplementary Figs. 22-25). The spatial distribution of resilience remains similar across methods (Supplementary Fig. 25), and the resilience differences among forest management types show nearly identical patterns (Supplementary Figs. 23 and 24). Importantly, the resilience gap between PF and NF is strongly correlated across the three approaches (Supplementary Fig. 22), indicating that our main findings are robust to temporal aggregation, sensor choice, and the treatment of missing values. These results provide strong support to the findings presented in Fig. 2 and Fig. 3.

Effect of normalization/standardization on resilience estimation: Standardization of vegetation index data could influence resilience metrics. It is more likely to affect λVar, because standardization sets the standard deviation of the data to one. The standard deviation is an input to the λVar calculation[23]. Therefore, standardization may change the results. In our resilience estimation, we did not normalize the anomaly data. To test whether normalization affects the results, we carry out the following analyses.

Here we focus on its effect on λAR1. We compare λAR1 derived from three kNDVI time series: (1) an anomaly series, obtained by subtracting the multi-year mean of each month from the corresponding monthly value; (2) a standardized series, where each monthly value is expressed as its deviation from the multi-year monthly mean divided by the corresponding multi-year monthly standard deviation (Z-scores); and (3) a normalized anomaly series, where each monthly anomaly is further rescaled to the [0,1] range using the minimum and maximum anomalies of the same month. Here are the related equations:

$$kNDVI\ anomaly = kNDVI - kNDVI_{mean} \quad (1)$$

$$kNDVI\ Z - scores = \frac{kNDVI - kNDVI_{mean}}{kNDVI_{std}} \quad (2)$$

$$Normalized\ kNDVI\ anomaly = \frac{(kNDVI - kNDVI_{mean}) - (kNDVI_{min} - kNDVI_{mean})}{(kNDVI_{min} - kNDVI_{mean}) - (kNDVI_{max} - kNDVI_{mean})} \quad (3)$$

Where $kNDVI_{mean}$, $kNDVI_{std}$, $kNDVI_{min}$ and $kNDVI_{max}$ denote the multi-year monthly mean, standard deviation, minimum, and maximum, respectively, for the corresponding month; Where kNDVI is the values for a specific month. Then, we apply the moving-window algorithm to compare differences in λAR1 between PF and NF.

Results show that the spatial distributions of λAR1 based on kNDVI Z-scores, kNDVI anomaly, and normalized kNDVI-anomaly are similar (Supplementary Fig. 26). The $\Delta\lambda$AR1-$kNDVI_{(PF,\ NF)}$ shows negative correlation with the P/PET by all three datasets, which is aligned with the findings of Fig. 3. This indicates that the normalization/standardization has minimal impact on the key findings.

Supplementary Note 5: Sensitivity tests on datasets uncertainty

Uncertainty of the reference forest management map. Because only a few global forest management datasets are currently available, we cannot perform a parallel re-analysis using alternative products. Instead, we can assess the reliability of GFMD using categorical accuracy maps. Specifically, we exclude pixels with low classification confidence by applying three verification thresholds (50%, 60%, and 70%). We then compare the resilience differences among forest management types using the moving-window method. The results consistently show similar patterns in resilience differences among managed forests across various thresholds, which are also in line with the patterns presented in Fig. 2 (Supplementary Figs. 27 and 28). These results indicate that our conclusions are robust. Additionally, the GFMD map has been validated by crowdsourced samples, with classification accuracy ranging from 60% to 80%[12,24]. GFMD does not incorporate three-dimensional vegetation structure, which is strongly affected by forest management practices[13,25]. As remote sensing technologies becoming advanced, higher-accuracy forest management datasets that capture structural information allow more rigorous validation of our results.

Influence of vegetation index spatial resolution on resilience estimation: The spatial resolution of vegetation indices may affect the estimation of resilience metrics. To assess this, we repeat our analysis using 500 m resolution data. For the vegetation datasets, the original datasets for GPP_PML, GPP_MODIS, LAI, and FPAR are provided at 500 m resolution, whereas NDVI (kNDVI) is available at 1 km resolution. For the sensitivity test, we instead employ the MOD13A1 and MYD13A1 datasets, which provide NDVI at 500 m and 16-day intervals, and aggregate them to monthly values using the Maximum Value Composite (MVC) method. Notably, the GFMD and GHFC datasets are also resampled to 500 m to match the spatial resolution of the vegetation indices. Based on these 500 m vegetation indices, GFMD, and GHFC data, we recalculate resilience metrics and apply the moving-window algorithm to compare resilience differences between PF and NF.
The results show that the spatial distributions of λAR1 at 500 m and 1000 m resolutions are very similar, as demonstrated for tropical forests in Africa (Supplementary Fig. 29). The $\Delta\lambda AR1_{(PF, NF)}$ shows negative correlation with the P/PET at both 500 m and 1000 m resolutions across all five vegetation indices (Supplementary Fig. 29), aligning with the findings in Fig. 3. These findings indicate that the main findings are robust to variability in spatial resolution. A previous study has reported that varying spatial resolution has minimal impact on the long-term estimation of ecosystem resilience[23].

Impact of vegetation index's time span and temporal frequency on resilience estimation:
The vegetation index's time span and temporal resolution might also influence resilience estimation. We conduct sensitivity tests using 16-day (MOD13A2, Terra) and monthly (MOD13A3, Terra) kNDVI datasets at 1 km spatial resolution. We estimate AR1 metrics over different time spans: 2001–2010, 2001–2015, 2001–2020, and 2001–2024. We then apply the moving-window algorithm to compare resilience differences between PF and NF. Results show that the $\Delta AR1\text{-}kNDVI_{(PF, NF)}$ shows negative correlation with the P/PET across various time spans and temporal frequencies (Supplementary Fig. 30). These results suggest that our findings are not strongly affected by the time span or frequency of the VIs data.

In addition, we note that the data used for resilience estimation covers the period 2001–2015, whereas overlaying 2015 GFMD and 2000 GHFC ensures the continuous and stable forest management in 2000–2015. Thus, there is a slight temporal mismatch between the two datasets. However, our sensitivity tests indicate that the length of the time series used for resilience estimation has minimal effect on the main results (Supplementary Fig. 30), which is consistent with previous studies showing that resilience indicators are robust to moderate changes in time-series length[23].

Supplementary Note 6: Sensitivity test by crowdsourced datasets

We further conduct our analysis using 210,000 locations provided by Lesiv et al.[12], which have been validated through expert review on the Geo-Wiki platform. These point data represent different forest management types in 2015. To ensure consistency in managed forest type over time, we exclude points that are classified as non-forested in 2000 based on Hanssen's map (GHFM), resulting in a final dataset of 140,000 locations. Resilience indicators (i.e., AR1-LAI) and P/PET are directly extracted for these locations. The results show that resilience decreases with increasing P/PET across different managed forest types (Supplementary Fig. 31), consistent with previous studies[11,26]. More importantly, we find similar evidence that human management reduces forest resilience (Supplementary Fig. 31). Specifically, planted forests with short rotation cycles (≤15 years) exhibit significantly lower resilience than unmanaged natural forests. Unmanaged natural forests display higher resilience than managed natural forests. These findings are aligned with those obtained from the paired-grid method (Fig. 2).

Building on the above-mentioned analysis, which initially controlled for the climatic variable P/PET, we further employ a nearest-neighbor method (similar to the paired-grid method) to match different forest management types and compare their resilience. In this method, each forest type is matched with its 15 closest counterparts from another type ($k = 15$). Results confirm that human management reduces forest resilience, with the strongest reduction observed under intensive management (Supplementary Fig. 32). Specifically, the largest resilience difference is observed in NF WOM vs. Plantations (ΔAR1-LAI $_{(\text{Plantations,NF WOM})}$ > 0.06), followed by NF vs. Plantations (ΔAR1-LAI $_{(\text{Plantations,NF})}$ > 0.05), NF WOM vs. F WM ($\Delta\lambda$AR1-LAI $_{(\text{F WM, NF WOM})}$ > 0.03), and then NF vs. PF (ΔAR1-LAI $_{(\text{PF,NF})}$ > 0.02).

Additionally, in drier regions, PF exhibit lower resilience than NF, whereas in more humid regions the opposite pattern emerges (Supplementary Fig. 33). Sensitivity tests with different k values (5, 10, and 15) produce similar patterns. However, some inconsistencies remain between the results based on crowdsourced points and those derived from GFMD. For instance, ΔAR1-LAI $_{(\text{PF, NF})}$ becomes positive only when P/PET < 2.5 (Supplementary Fig. 33), whereas Fig. 3 suggests the threshold is P/PET < 1.5. This discrepancy is potentially due to the imbalance of samples in the crowdsourced points, where samples of forest management types like PF (N_{PF} = 8357) are fewer than those for NF ($N_{NF\ WOM}$ = 39534 and $N_{NF\ WM}$ = 82358) [24,27]. This highlights a limitation of the crowdsourced point dataset and suggests that further improvements in the accuracy of forest management maps are needed for more balanced comparisons.

Supplementary Note 7: The relation between resilience and tree species richness

We conduct a preliminary investigation into the relationship between forest resilience and tree species richness. Our objective is to understand how diversity might modulate resilience across different forest management types and climatic gradients. Tree species richness data at a 0.025° resolution are derived from GFDD (Global forest diversity dataset)[28,29], and are resampled to 1 km to match the resolution of vegetation datasets. For each crowdsourced location, we extract P/PET, resilience indicators (AR1-LAI), and tree species richness. We first analyze the relationship between AR1-LAI and tree species richness across different forest management types. The results show that greater tree species richness can lead to a decrease in AR1-LAI (i.e., an increase in resilience) (Supplementary Fig. 31 g-l). The strongest negative relationship is found in long-rotation and short-rotation PF, with the lowest slopes of -0.0020 and -0.0016, respectively. This finding suggests that increasing tree species diversity in afforestation could be a viable strategy to enhance forest resilience.

To provide a more comprehensive view, we create bivariate heatmaps to investigate how AR1-LAI responds to the combined effects of climate (P/PET) and tree species richness (Supplementary Fig. 31 m–n). This method allows us to identify specific conditions where the relationship between resilience and diversity might change. The results reveal that the influence of species richness on resilience is highly dependent on climate, with different patterns emerging in drier versus more humid regions. Specifically, in drier regions (P/PET < 1.19), increasing species diversity has a minimal effect on enhancing resilience. In contrast, in more humid regions, a higher tree species diversity is significantly associated with greater resilience. These exploratory findings provide initial evidence that integrating biodiversity considerations into forest management, particularly in humid climates (and for planted forests), could enhance forest resilience.

Supplementary Note 8: The limitations of applying the early-warning indicators

Early warning indicators (EWI, e.g., λAR1 and λVar) are to be interpreted as a measure of an approaching tipping point[30,31]. In systems that lack such critical transition, a decline in resilience does not necessarily imply an approaching tipping point. This study focuses on global forest ecosystems. Previous studies reported that some regions such as the Amazon, temperate forests, and boreal forests have exhibited signs of degradation or structural transition under disturbances such as fire and drought[32–35]. These regions are expected to experience further large-scale transformations in the future due to ongoing warming[36,37]. Confirming the widespread occurrence of critical transitions in global forests would strengthen the case for using EWI as a measure of proximity to tipping points.

In systems without tipping points, elevated EWI values can still indicate a loss of system resilience. EWI have physical interpretations related to system resilience. For example, an increase in AR1 reflects stronger memory of past states, meaning that previous disturbances continue to influence the present[38]. This suggests a reduced ability of the system to absorb disturbances and maintain its equilibrium state. In this study, we used the EWI to explain resilience difference across managed forests.

Satellite remote sensing serves as a data source for the calculation of EWI. To ensure the reliability of EWI estimation, long-term and high-frequency satellite datasets are essential. The observation period should be sufficiently long, and the sampling frequency adequately high. For the sampling frequency, interpolation used to fill data gaps, which is common in satellite records, may interfere with the EWI estimation[23,39]. Moreover, the choice of sampling frequency should be aligned with the intrinsic dynamics of the system. For forest ecosystems, where structural changes typically occur over annual timescales, monthly satellite observations are generally adequate. In this study, we also conducted sensitivity tests on both temporal (Supplementary Fig. 30) and spatial resolutions (Supplementary Fig. 29) to assess the robustness of the EWI estimation.

Sensor degradation and replacement present further challenges[40]. It is often difficult to obtain long-term data from a single satellite sensor. Merging datasets from multiple sensors can extend time series, but may also alter the signal-to-noise ratio. This may bias EWI estimates. For instance, newer sensors often produce higher signal-to-noise ratios, potentially increasing λAR1 and lowering λVar values. To address this, we compared EWI derived from single-sensor and multi-sensor data (Supplementary Figs. 22-25). We also used both λAR1 and λVar for cross-validation (Figs. 2~5). These sensitivity tests confirmed the robustness of our findings.

Overall, in this study, the integration of multiple EWI, combined with rigorous sensitivity analyses, supports the reliability of satellite-based approaches for comparing ecological resilience across different forest management types.

Supplementary Note 9: The relation between early-warning indicators, tipping point, and resilience.

There are two main definitions of resilience in ecological research[41]. Engineering resilience describes a system's ability to recover rapidly following a specific, intense disturbance (e.g., wildfire, drought, or logging), with emphasis on the speed of return to a reference state[42]. In contrast, ecological resilience refers to a system's capacity to resist (or absorb) changes, maintain its present structure even under a series of disturbances of varying intensity[39,43–45]. In this study, we adopt the ecological resilience perspective, which better captures the reality that managed forests are subject to a series of disturbances over time rather than specific and intense shocks.

We quantify ecological resilience using indicators such as AR1 (lag-1 autocorrelation), interpreted as early warning signals of declining stability under the framework of critical slowing down (CSD)[38,46,47]. Systems with lower resilience reflect higher AR1 values as disturbances leave longer memory traces in the time series, indicating reduced capacity to absorb shocks. Conversely, highly resilient systems dissipate disturbance effects rapidly, exhibiting low AR1 values.

These indicators are also known as early warning indicators because, according to CSD theory, they provide signals of impending irreversible shifts in a system's state. Many of the real-world systems are non-linear systems with explicit thresholds[31,41]. They often experience irreversible shifts once these thresholds are crossed. Specifically, at the beginning, when the environment changes, the system changes according to the State-1 curve. When the environment condition reaches the threshold, the system suddenly jumps to the other stable state (from State-1 to State-2). When the environmental conditions further change, the system no longer changes along the state 1 curve, but along a new curve (the State-2 curve) (Supplementary Fig. 35a). That jump marks the tipping point. Such a jump is often irreversible. In the context of our study, the tipping point is defined as a theoretical threshold at which the high-density closed-canopy forests would lose their resilience and potentially shift toward an alternative state such as low-density forests[48]. Although PF and NF currently exhibit similar states in photosynthesis, PF generally possess lower structural complexity and shallower, simplified root systems[49]. These characteristics reduce their ability to absorb external disturbances, making them more prone to crossing the tipping point and transitioning toward low-cover, open forests under continued disturbances. In contrast, NF, with their higher structural complexity and well-developed root systems, tend to maintain their initial high-cover, closed-canopy state due to stronger self-regulation and resilience.

Then, we use the concept of attraction basins to illustrate how shifts between stable states are related to early warning indicators. Each state of the system is represented by a basin, and transitions between stable states are depicted as the ball moving from one basin to another (when crossing the tipping point)[31]. The depth and steepness of the attraction basin indicate the system's resilience: a deeper and steeper basin means the system can absorb perturbations more effectively, reflecting higher resilience. For example, in State-1, where the basin is deep, the system (the ball) returns rapidly to its equilibrium position after a disturbance, resulting in small and short-lived fluctuations around the mean state. This reflects high resilience and is expressed in the time series by low autocorrelation (AR1) and variance (Supplementary Fig. 35b). In contrast, in State-2, the attraction basin becomes shallower and flatter. Here, the system's resilience is lower, leading to larger deviations from the average state and more prolonged fluctuations (Supplementary Fig. 35c).

Although the system may eventually return to equilibrium, the process takes much longer, indicating low resilience. In the time series, this is reflected as higher autocorrelation (AR1) and variance, signaling that the system retains the effects of past disturbances for a longer period ("longer memory")[38].

As the system moves from State-1 toward State-2 and approaches the tipping point, the basin of State-1 continues to become shallower and flatter (Supplementary Fig. 35d). This makes it easier for even minor disturbances to push the system out of its current state, as its sensitivity to perturbations increases[31,38,39]. The progression from a deep to a shallow basin is characterized by a gradual loss in resilience (e.g., high to low resilience), increasing variance and autocorrelation in the system's dynamics (i.e., critical slowing down). These changes serve as early warning signals for reduced resilience and impending regime shifts.

Our analysis of LAI anomaly (after detrending and deseasonalization) in two types of forests provides support for the theoretical concepts of resilience and critical slowing down. Specifically, planted forests with short rotation periods (years < 15) exhibit higher AR1 values than nearby managed natural forests (Supplementary Fig. 36). This relatively higher AR1 value suggests that the LAI of planted forests retains the effects of past disturbances for a longer period—indicating a "longer memory" (Supplementary Fig. 36 c, e). In contrast, LAI anomalies in managed natural forests tend to dissipate more rapidly, implying a shorter memory and higher ecological resilience (Supplementary Fig. 36 d, f). These observations align with the CSD theory, suggesting that the rotational management practices in planted forests may reduce ecological resilience.

Supplementary Note 10: The quantification of λAR1 and λVar

λAR1 and λVar are based on the Ornstein–Uhlenbeck process. This process describes the natural tendency of a system to revert to equilibrium after perturbations, making it a robust tool for analyzing resilience dynamics. The Ornstein–Uhlenbeck process can be described by the following analytical formulation:

$$dX_t = \lambda X_t dt + \sigma dW \quad (4)$$

where X_t represents the value of the state variable at time t; W denotes a Wiener process serving as the stochastic driving force in the system; and σ represents the amplitude of this noise. For stable dynamics, λ is less than 0, whereas an increasing (decreasing) λ indicates a loss (gain) of resilience. In this study, the time step dt is set to 1, corresponding to the monthly temporal resolution. The Ornstein–Uhlenbeck process can be expressed in lag-1 autoregressive form (i.e., from continuous to discrete form) as follows:

$$X_{n+1} = aX_n + \epsilon_n \quad (5)$$

where X_{n+1} denotes the system state at discrete time step $n+1$ (where X_n is the system state at discrete time step n). Therefore, a represents the regression coefficient between X_n and X_{n+1} (lag-1 autoregression), whereas ϵ_n is the discrete driving noise (e.g., residuals)**.** Thus, the autocorrelation at lag n can be derived as follows:

$$a(n) = e^{\lambda n \Delta t} \quad (6)$$

Furthermore, based on exact discretization of the Ornstein–Uhlenbeck process and Itô isometry[22], the variance of the discrete driving noise is calculated by the formula:

$$Var[\epsilon_n] = \emptyset^2 = -\frac{\sigma^2}{2\lambda}(1 - e^{2\lambda\Delta t}) \quad (7)$$

The variance of the full discretized time series of the state variable X can be expressed as follows:

$$Var[X] = \frac{\emptyset^2}{1-e^{2\lambda\Delta t}} = -\frac{\sigma^2}{2\lambda} \quad (8)$$

Based on the above equations, *λAR1* and *λVar* can be calculated as follows:

$$\lambda AR1 = \frac{1}{\Delta t} \log(a) \quad (9)$$

$$\lambda Var = \frac{1}{2\Delta t} \log\left(1 - \frac{\emptyset^2}{Var[X]}\right) \quad (10)$$

We note that the λAR1 and λVar equations may result in null values due to logarithmic constraints (i.e., AR1 < 0 or $\frac{\emptyset^2}{Var[X]}$>1). In this case, λAR1 or λVar is treated as *NA* and excluded from spatial and temporal statistics.

Supplementary Fig. 1~Fig. S36:

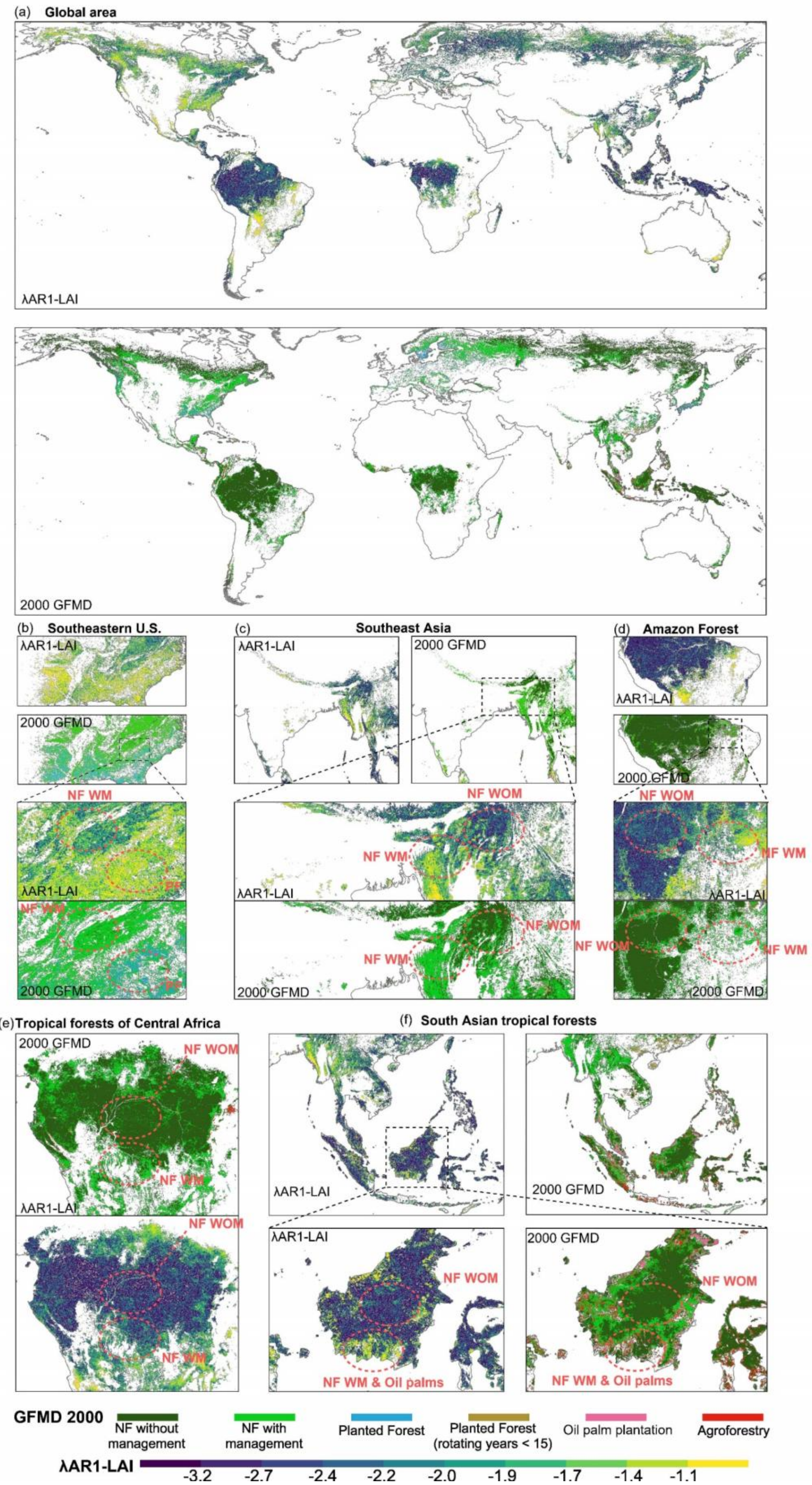

Supplementary Fig. 1. Spatial distribution of forest resilience (λAR1–LAI) and management types from the Global Forest Management Dataset (GFMD 2000). Higher λAR1–LAI values indicate lower resilience. (a) Global distribution of forest resilience and management types. (b–f) Regional examples highlight contrasting resilience patterns among different forest management types. (b) In the Southeastern United States, planted forests (PF) exhibit lower resilience (higher λAR1–LAI) compared with nearby managed natural forests (NF WM). (c) In Southeast Asia, managed natural forests (NF WM) show lower resilience than unmanaged natural forests (NF WOM). (d) In the Amazon, reduced resilience is observed along forest edges where NF WM exhibit lower resilience than adjacent NF WOM. (e) In Central Africa, NF WM also show lower resilience than NF WOM. (f) In South and Southeast Asia, oil palm plantations and managed natural forests (NF WM and oil palms) exhibit substantially lower resilience than unmanaged natural forests. Flesh circles indicate representative regions used to illustrate contrasting resilience patterns. Color bars represent (top) λAR1–LAI values and (bottom) forest management categories from GFMD 2000, including NF without management (NF WOM), NF with management (NF WM), planted forest (PF), planted forest with rotation years <15, oil palm plantation, and agroforestry.

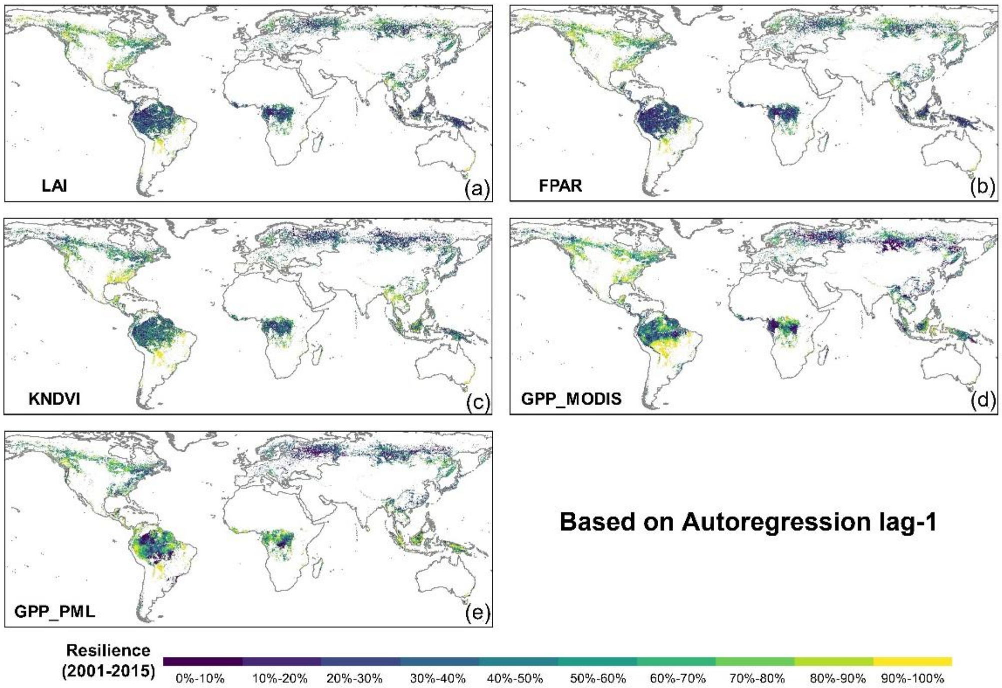

Supplementary Fig. 2. The spatial distribution of forest resilience (AR1) estimated by five vegetation indices: (a) LAI, (b) FPAR, (c) kNDVI, (d) GPP_MODIS, (e) GPP_PML, displaying similar patterns. The maps show the global percentile-based distribution of AR1 during 2001–2015, where higher percentile values indicate greater AR1 (lower resilience).

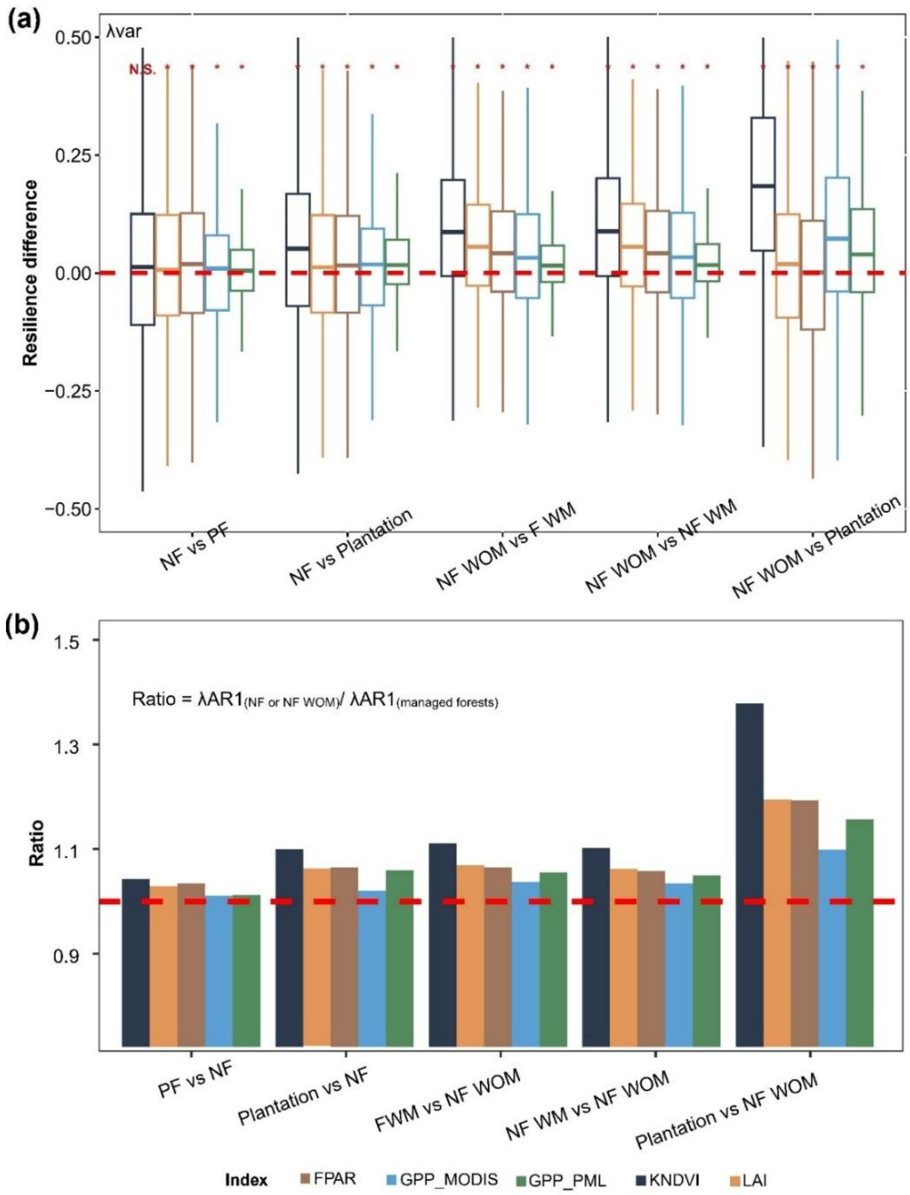

Supplementary Fig. 3. (a) Boxplots of resilience differences (ΔλVar) between different forest management types, including NF vs PF (n=8220), NF vs Plantations (n=12860), NF WOM vs F WM (n=34196), NF WOM vs NF WM (n=35578), and NF WOM vs Plantations (n=959). Results are shown for five vegetation indices (FPAR, GPP_MODIS, GPP_PML, kNDVI, and LAI). The y-axis represents the difference in resilience (ΔλVar) between two forest management types (e.g., NF vs PF), where a positive ΔλVar indicates higher resilience (i.e., lower AR1) in the first forest type (NF). Asterisks (*) indicate significant differences ($p < 0.05$), while N.S. indicates non-significance. The red dashed line represents zero difference. Statistical significance was assessed using a two-sided Wilcoxon test to examine whether the resilience difference significantly differs from zero. (b) Ratios of λAR1 between different forest management types. The "Ratio" is calculated as the λAR1 of NF (or NF WOM) divided by the λAR1 of managed forests. The red line denotes a ratio of 1, and the bars represent the mean values. Ratio values greater than one show that λAR1 of natural forests is higher than that of managed forests, indicating lower resilience of managed forests.

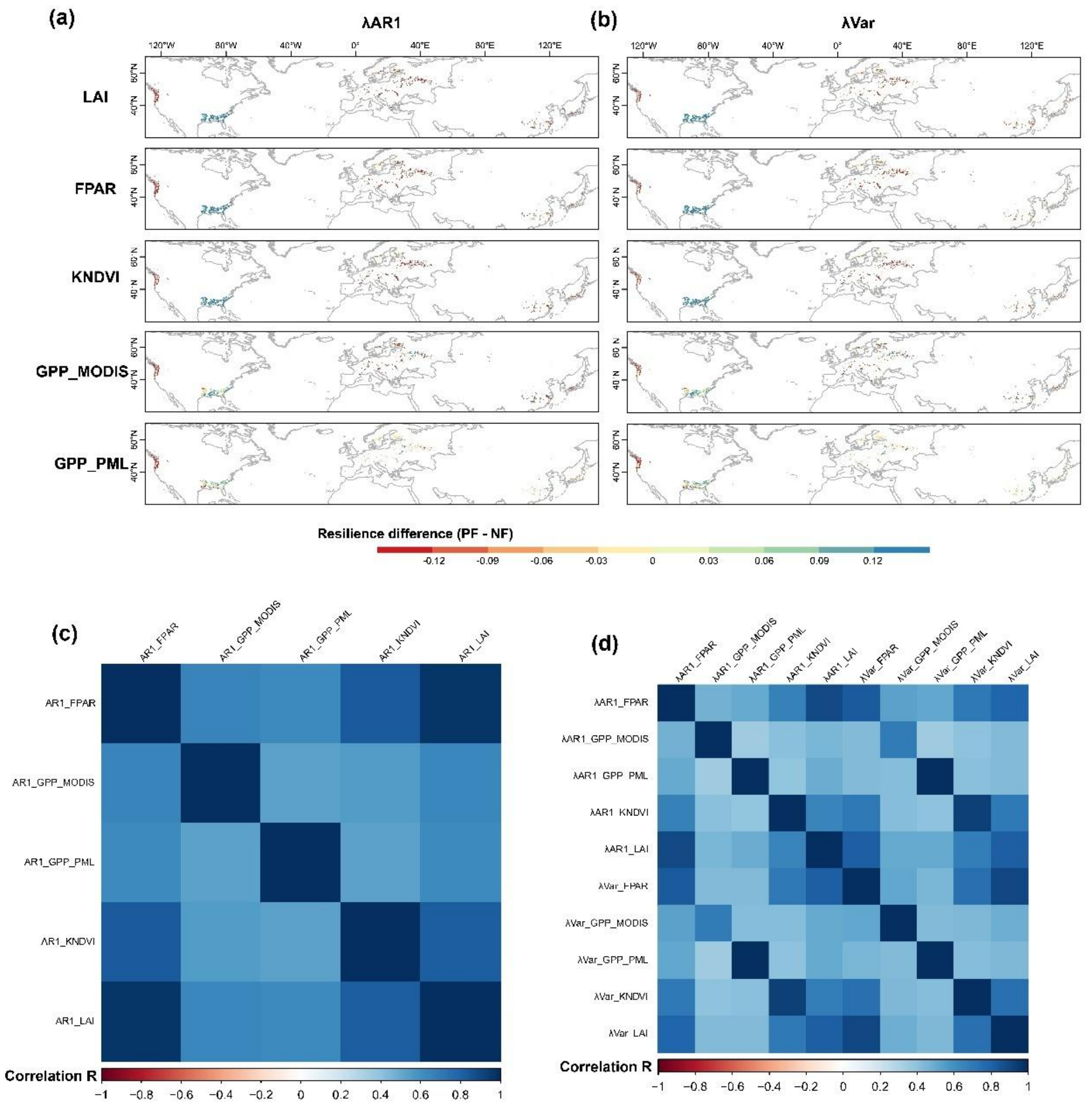

Supplementary Fig. 4. The vegetation resilience difference between PF and NF in paired grids. The spatial patterns of resilience difference estimated by λAR1 (a) and λVar (b) are displayed. Positive values in panels (a) and (b) indicate that PF have lower resilience than NF, that is, $\Delta\lambda AR1_{(PF, NF)} = \lambda AR1_{PF} - \lambda AR1_{NF} > 0$. The correlation matrix among the vegetation resilience differences calculated by combinations of resilience equations (AR1, λAR1, and λVar) and vegetation products (GPP_MODIS, GPP_PML, kNDVI, LAI, FPAR) is shown (c, d). “AR1_LAI” indicates the AR1 values by LAI index, and “λAR1_LAI” indicates the λAR1 values by LAI index.

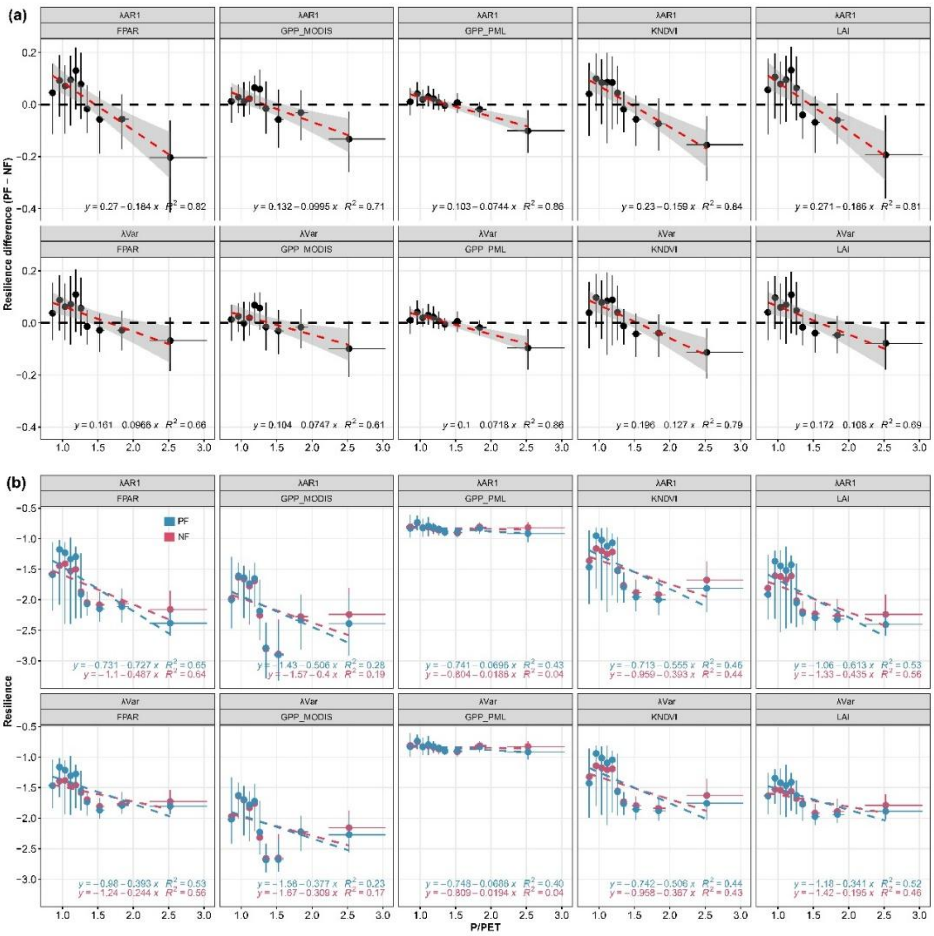

Supplementary Fig. 5. Resilience of PF and NF along dryness index gradients. (a) Relationships between the dryness index (P/PET, precipitation-to-potential evapotranspiration ratio) and resilience differences between PF and NF (e.g., ΔλAR1-LAI $_{(PF,\ NF)}$), estimated using five vegetation indices (FPAR, GPP_MODIS, GPP_PML, kNDVI, LAI). Each point corresponds to the mean value within a P/PET decile at the global scale (n = 822), with error bars indicating the 1st and 3rd quartile values. Regression lines with 95% confidence intervals are shown. (b) The resilience of PF and NF over the dryness index gradient.

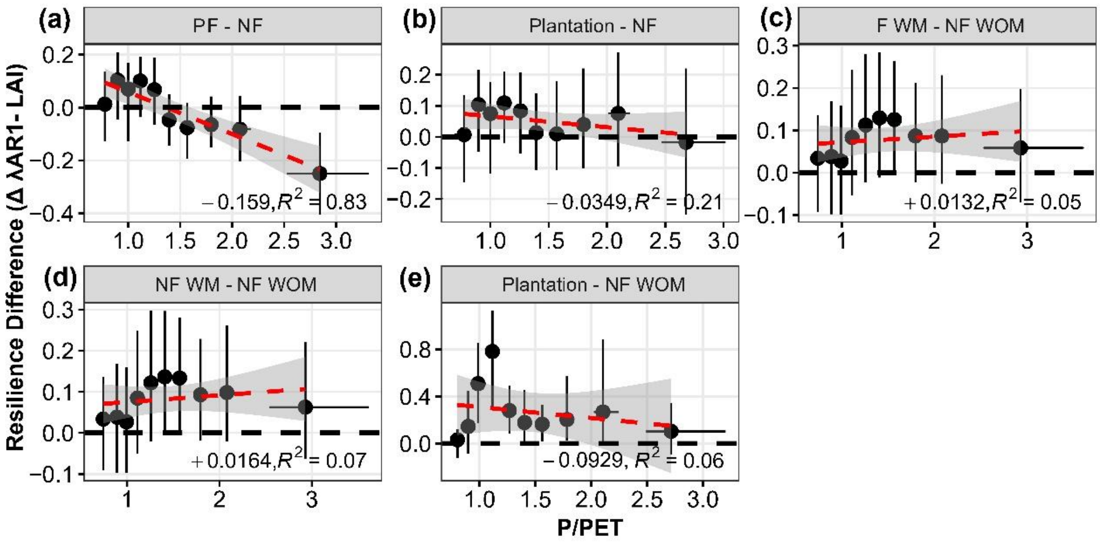

Supplementary Fig. 6. Relationship between climatic aridity (P/PET) and resilience differences (ΔλAR1–LAI) between paired forest management types. Panels (a–e) show comparisons among PF–NF, Plantation–NF, FWM–NF WOM, NF WM–NF WOM, and Plantation–NF WOM, respectively. Each point represents the global mean resilience difference within a P/PET decile, and vertical error bars indicate the interquartile range (25th–75th percentiles). Dashed red lines denote linear regression fits, with shaded grey areas showing the 95% confidence intervals. The horizontal dashed black line indicates zero difference in resilience.

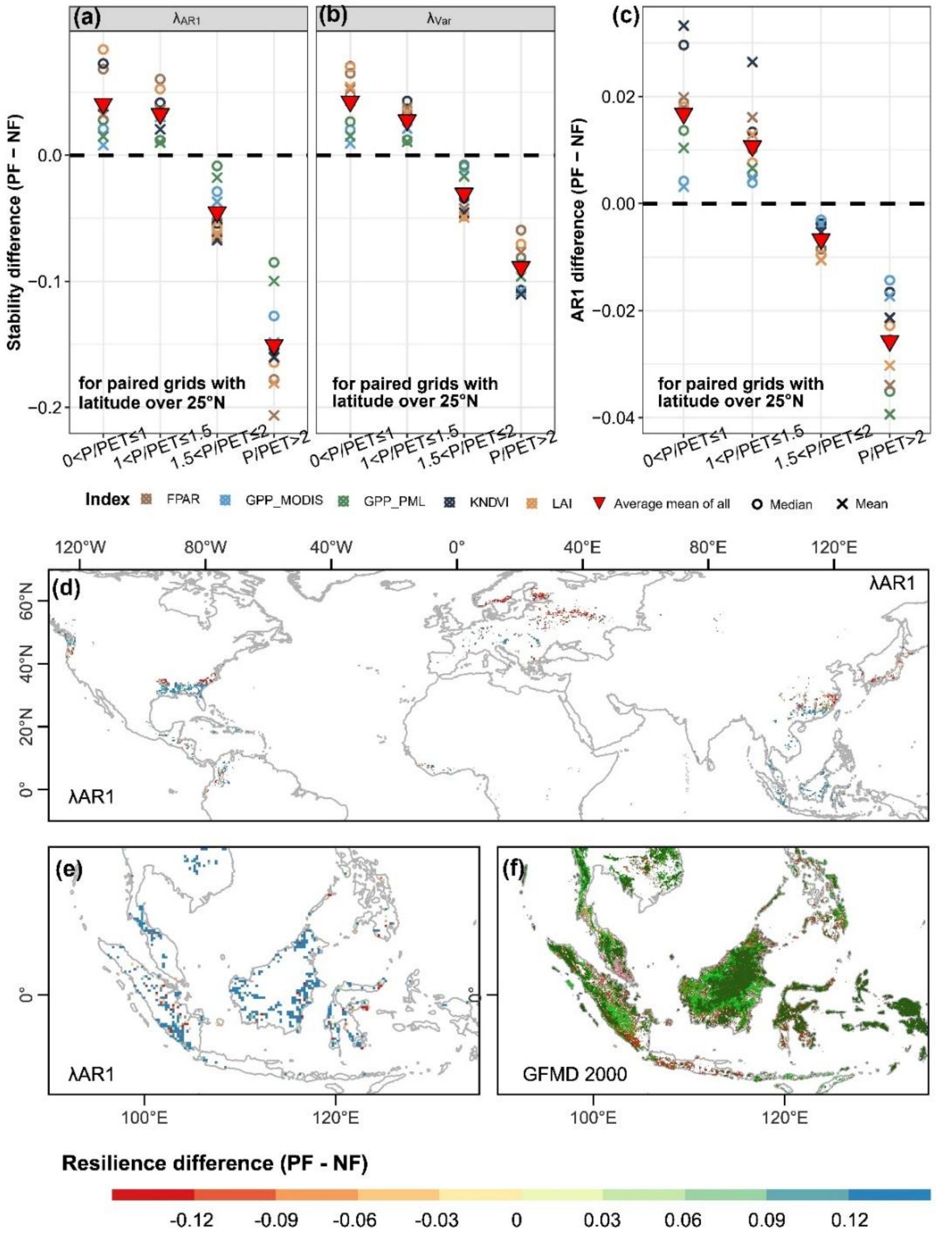

Supplementary Fig. 7. The resilience difference between PF and NF is based on the broad definition of planted forests. Compared to Fig. 3 in the main text, the term "PF" in Supplementary Fig. 7 is defined broadly, encompassing agroforestry, oil palms, planted forests with short rotations (year < 15 years), and planted forests with long rotations (year > 15 years) (i.e., all human planted trees). (a, b, c) The vegetation resilience differences between PF and NF are depicted alongside the dryness index gradient for latitude over 25 °N. (d, e, f) The spatial patterns of vegetation difference between PF and NF are illustrated. As the narrow definition of planted forests in the main text corresponds mainly to grid cells at latitudes above 25° N (Fig. 3), we apply the same latitude restriction in analyses (a–c), which showed patterns consistent with those in the main text.

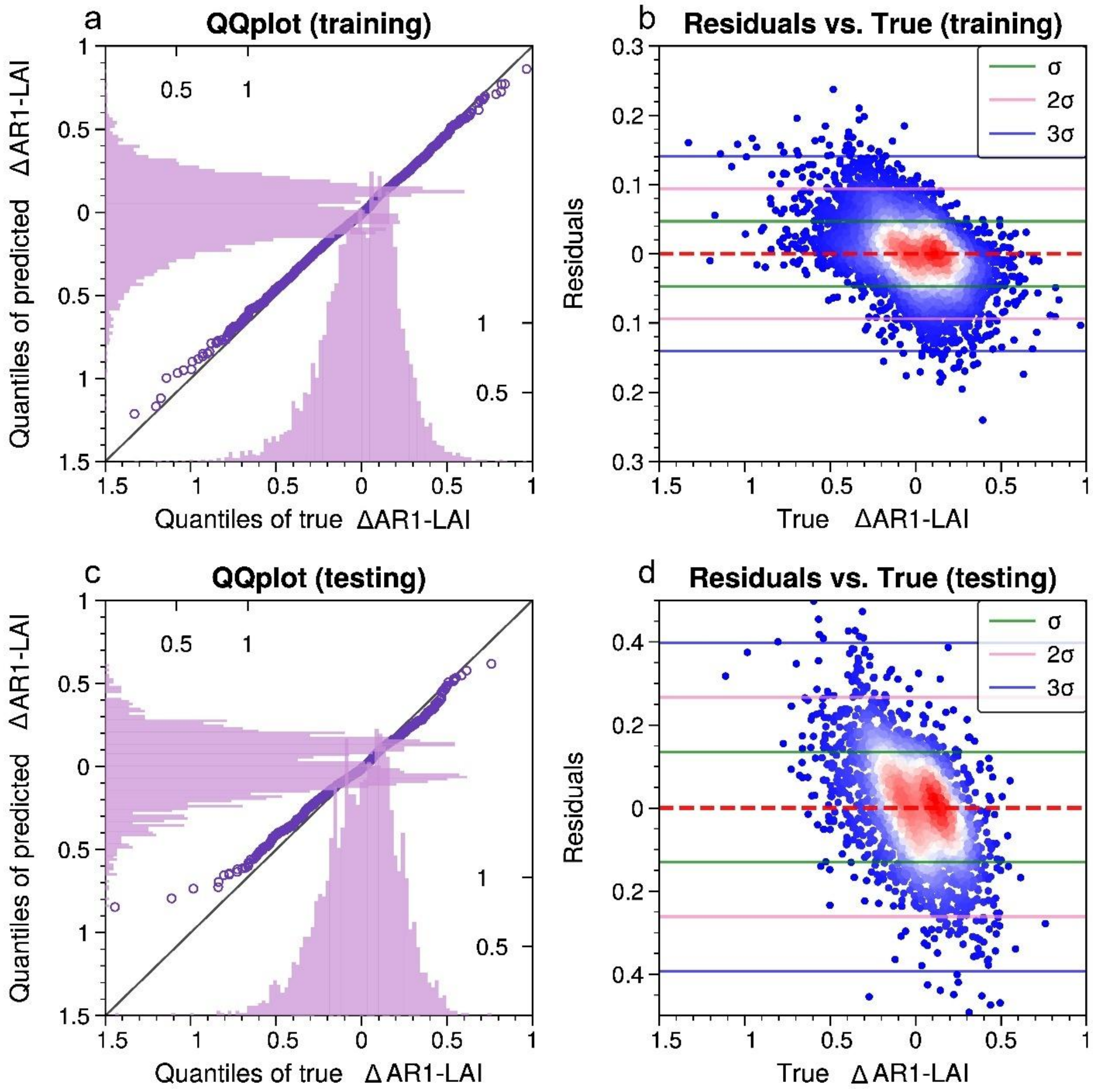

Supplementary Fig. 8. The performance of environmental factors on vegetation resilience difference between PF and NF. (a, c) The QQ-plot between true △λAR1-LAI $_{(PF, NF)}$ and predicted △λAR1-LAI $_{(PF, NF)}$ for the training and testing samples. (b, d) The scatter plots between true △λAR1-LAI $_{(PF, NF)}$ and the residuals of models for the training and testing samples are shown.

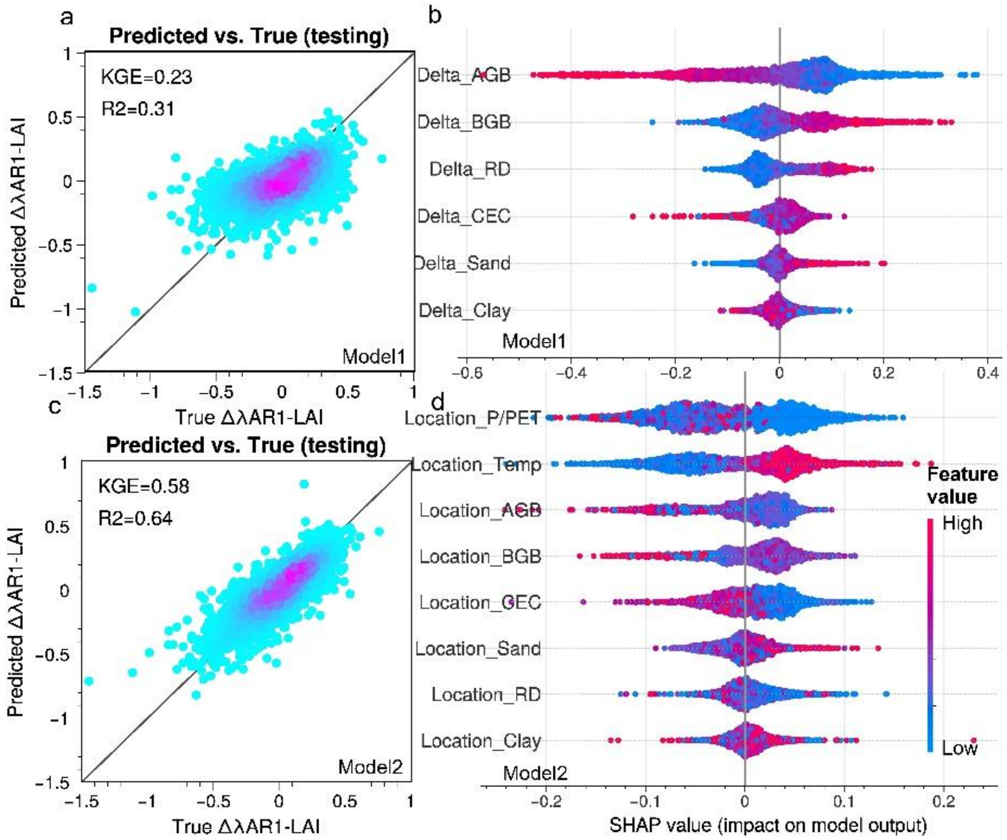

Supplementary Fig. 9. The performance of environmental factors on vegetation resilience difference between PF and NF in model 1 and model 2. Model 1 uses the background difference to predict the $\triangle\lambda$AR1-LAI$_{(PF, NF)}$, and Model 2 uses the local climate or soil background to predict the $\triangle\lambda$AR1-LAI$_{(PF, NF)}$. (a, c) True versus predicted $\triangle\lambda$AR1-LAI$_{(PF, NF)}$ for the testing samples. The coefficient of determination (R^2) and Kling-Gupta efficiency (KGE) are shown in labels. (b, d) The SHAP values of the environmental factors on the resilience difference. The red and blue colors signify the high and low values of the environmental factors, respectively. The SHAP value reflects the effect of variables on the resilience difference (e.g., positive or negative). For example, red points in temperature indicate a positive SHAP value, suggesting that a higher temperature background could enhance $\triangle\lambda$AR1-LAI$_{(PF, NF)}$. "Location_Factor" refers to the local background of the paired grid cells, while "Delta_Factor" represents the difference in environmental factors between PF and NF.

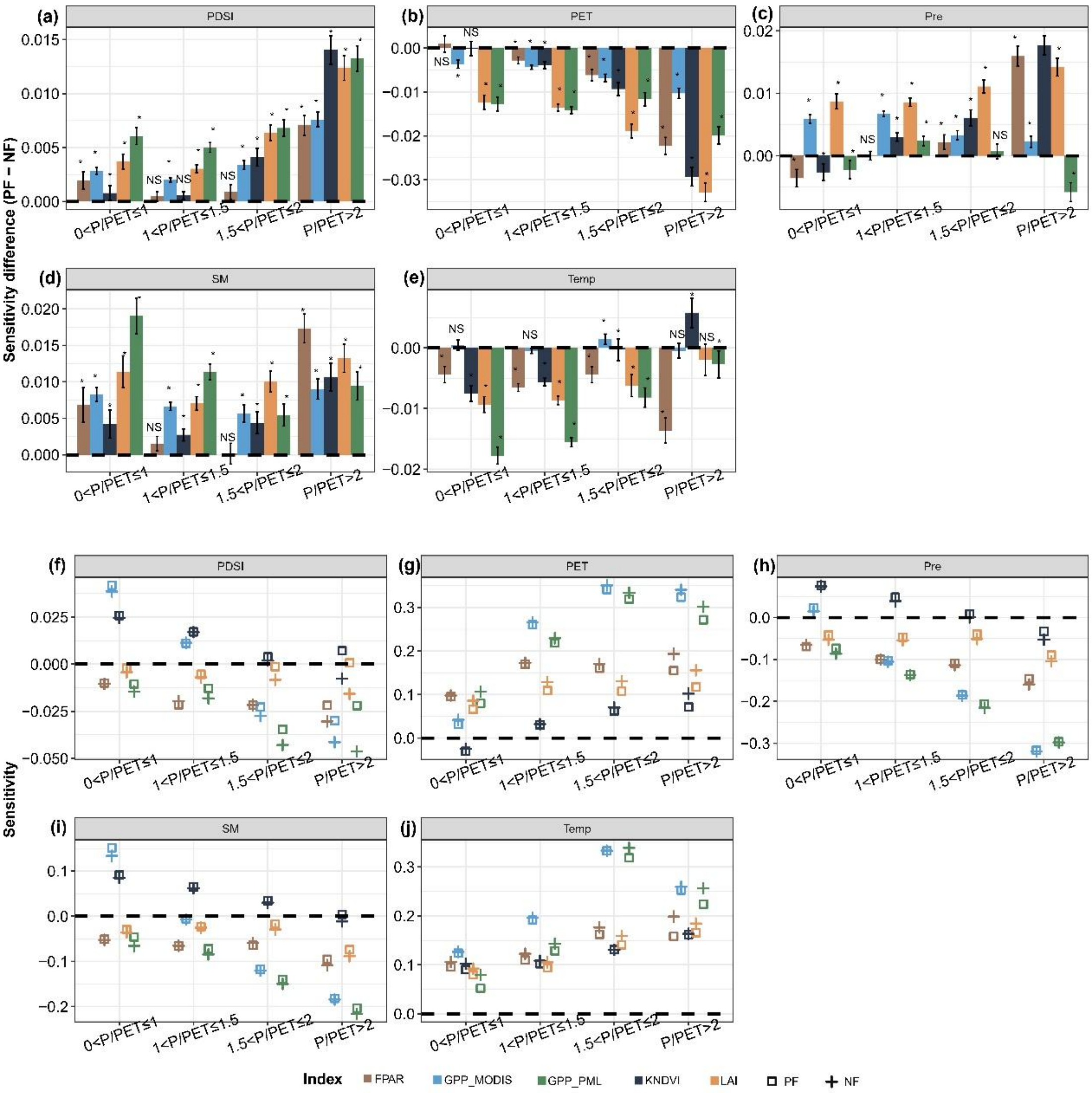

Supplementary Fig. 10. Sensitivity of PF and NF to climate variables across P/PET gradients. (a–e) Differences in climate sensitivity between PF and NF for (a) PDSI, (b) PET, (c) Precipitation (Pre), (d) Soil Moisture (SM), and (e) Temperature (Temp) across P/PET intervals. Bars represent sensitivity differences (PF – NF) based on five vegetation indices (FPAR, GPP_MODIS, GPP_PML, kNDVI, LAI). Error bars estimated by mean±2×standard error (SE). Statistical significance was assessed using a two-sided Wilcoxon test to examine whether the resilience difference significantly differs from zero. Asterisks (*) denote significant differences (p < 0.05), while NS indicates non-significance. (f–j) Sensitivity of PF and NF to the same climate variables across P/PET gradients. Results are presented separately for PF (□) and NF (+). Dashed lines indicate zero sensitivity.

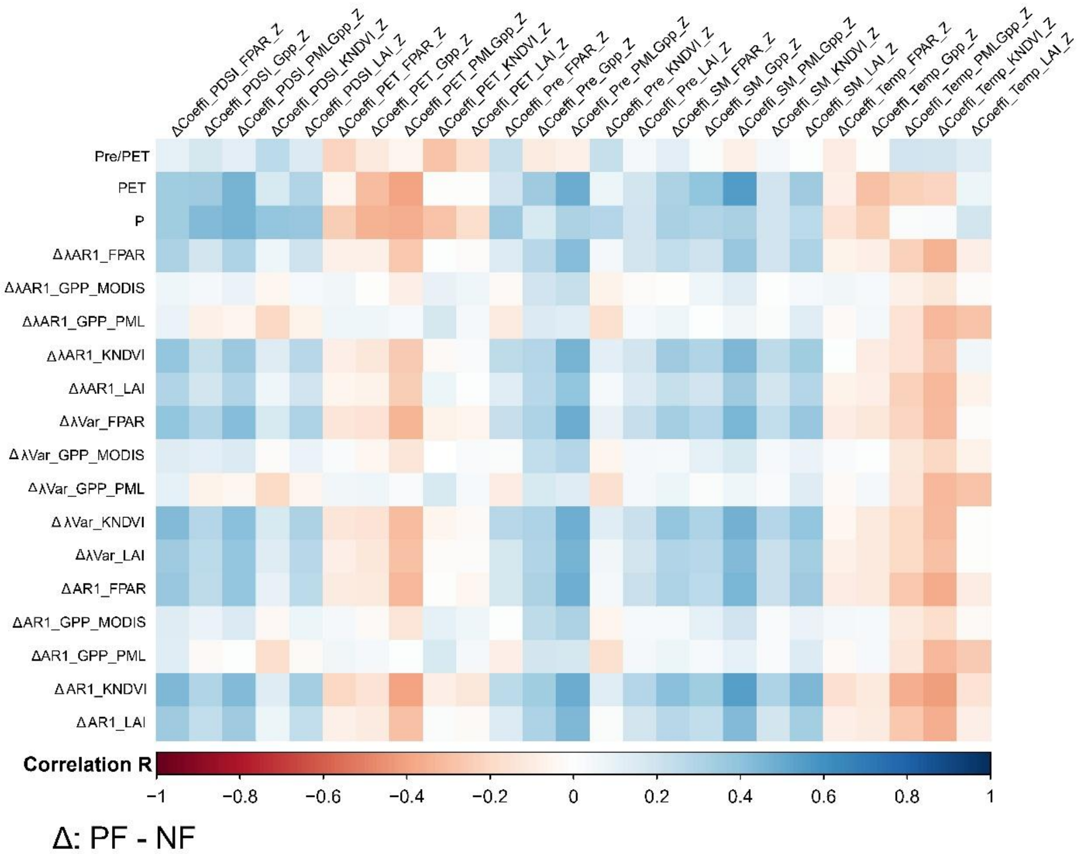

Supplementary Fig. 11. Correlation matrix between vegetation–climate sensitivity differences (PDSI, PET, Pre, SM, Temp) and resilience differences (AR1, λAR1, λVar) between PF and NF, derived from multiple vegetation indices (FPAR, GPP_MODIS, GPP_PML, kNDVI, LAI). Blue colors indicate positive correlations, while red colors indicate negative correlations. For example, "ΔλAR1_FPAR" represents the λAR1-FPAR difference between PF and NF, and "ΔCoeffi_PDSI_FPAR_Z" represents the PF-NF difference in the climate sensitivity of FPAR to PDSI (i.e., climate sensitivity).

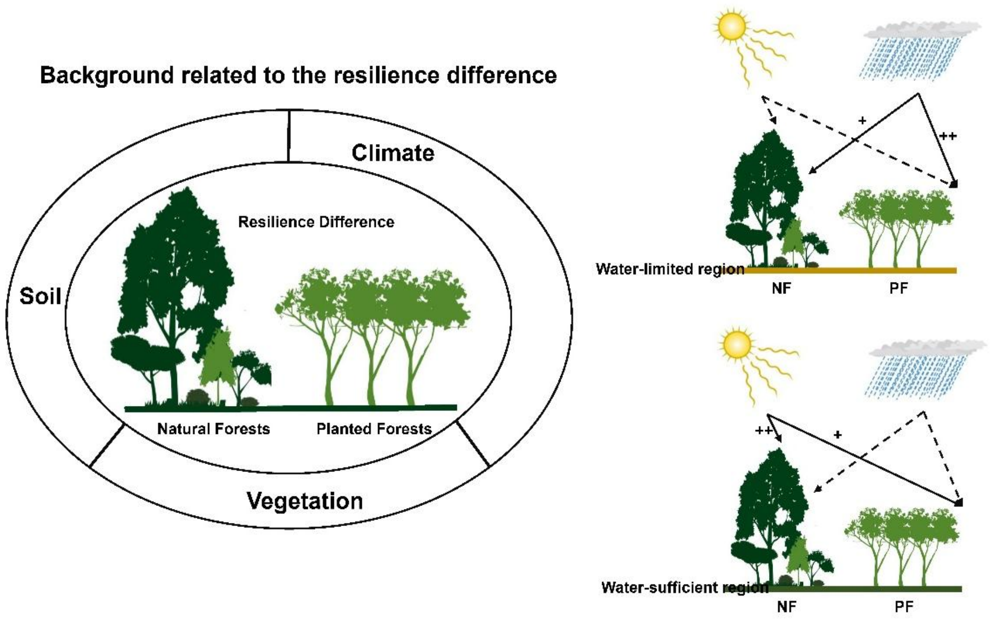

Supplementary Fig. 12. Conceptual diagram illustrating how resilience differences between PF and NF are shaped by local biophysical contexts, e.g., climate regions. In water-limited regions (dry areas), vegetation is highly sensitive to water (e.g., soil moisture and precipitation). PF show higher sensitivity to water stress than NF. This makes PF more vulnerable to drought, leading to larger biomass losses and lower resilience. Their higher sensitivity to water disturbances results in lower resilience. In water-sufficient regions (humid areas), vegetation is limited by energy (e.g., temperature). PF are less sensitive to energy-related changes than NF. This reduced sensitivity helps PF maintain stability and explains their higher resilience in these humid conditions.

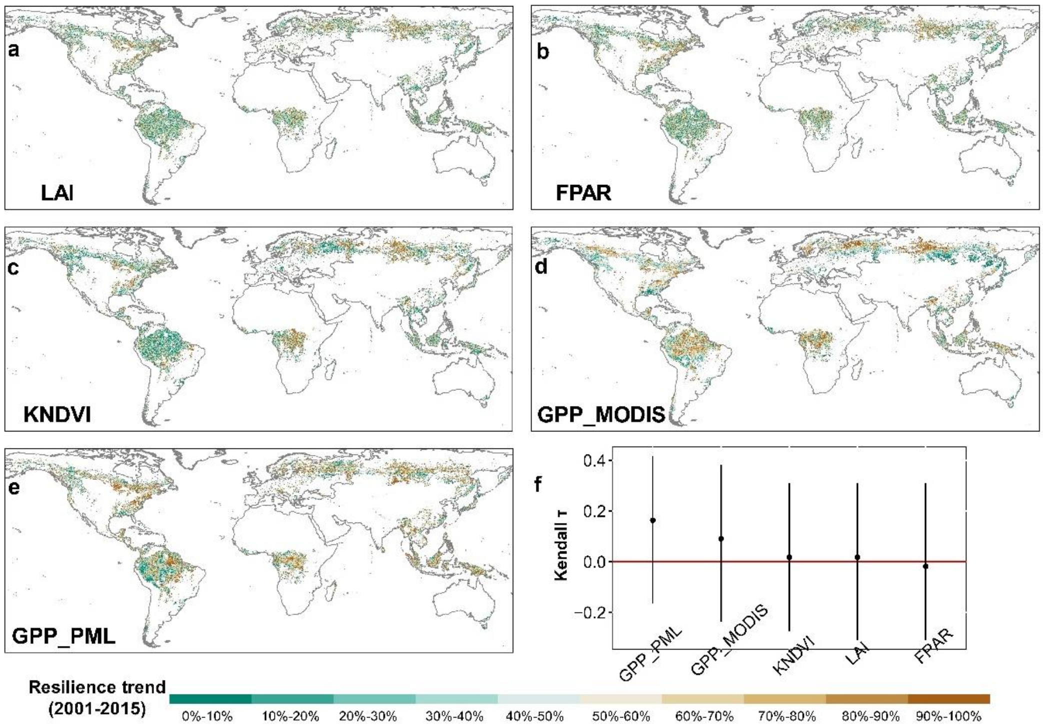

Supplementary Fig. 13. Spatial and statistical patterns of forest resilience (AR1-LAI) trends during 2003–2013 (based on the vegetation dataset from 2001 to 2015), estimated using a 4-year moving window. The trend of each pixel is estimated by Kendall's τ. Colors indicate quantile bins (10th–90th percentile) derived from the distribution of Kendall's τ values. (a–e) Maps show resilience trends derived from five vegetation indices: (a) LAI, (b) FPAR, (c) kNDVI, (d) GPP_MODIS, and (e) GPP_PML. (f) The point is the median Kendall's τ value, and the highest and lowest bar represents the 1st and 3rd quarter value.

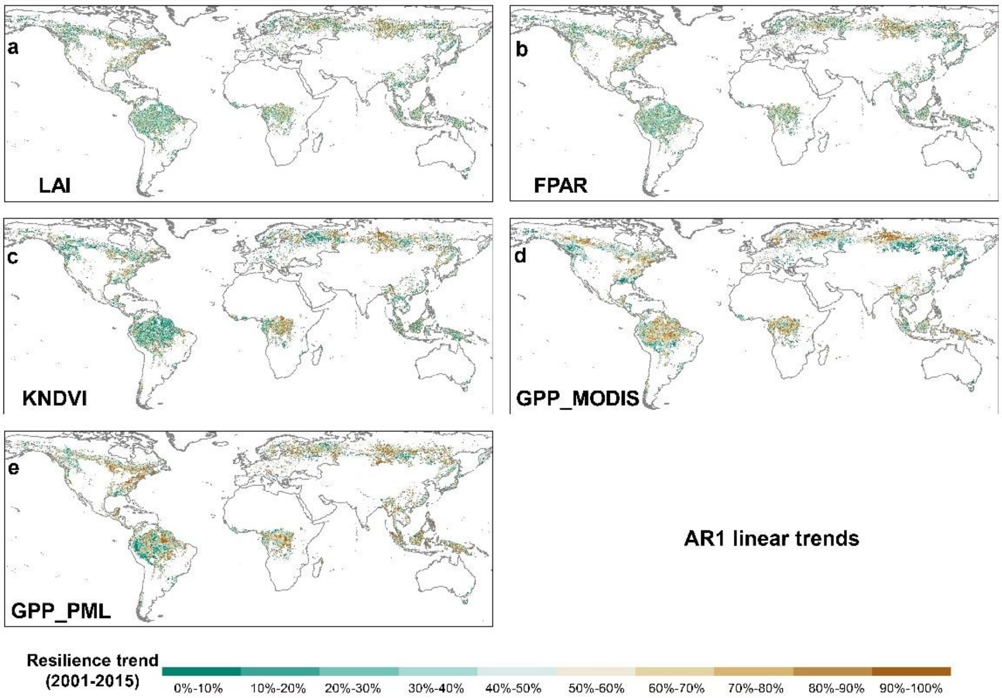

Supplementary Fig. 14. Spatial and statistical patterns of forest resilience trends (2003–2013) estimated by linear regression using a 4-year moving window. Similar to the Supplementary Fig. 13, but here the trends are estimated using linear regression. Colors indicate quantile bins (10th–90th percentile) derived from the distribution of long-term trends (i.e., regression slopes). (a–e) Maps show resilience trends derived from five vegetation indices: (a) LAI, (b) FPAR, (c) kNDVI, (d) GPP_MODIS, and (e) GPP_PML.

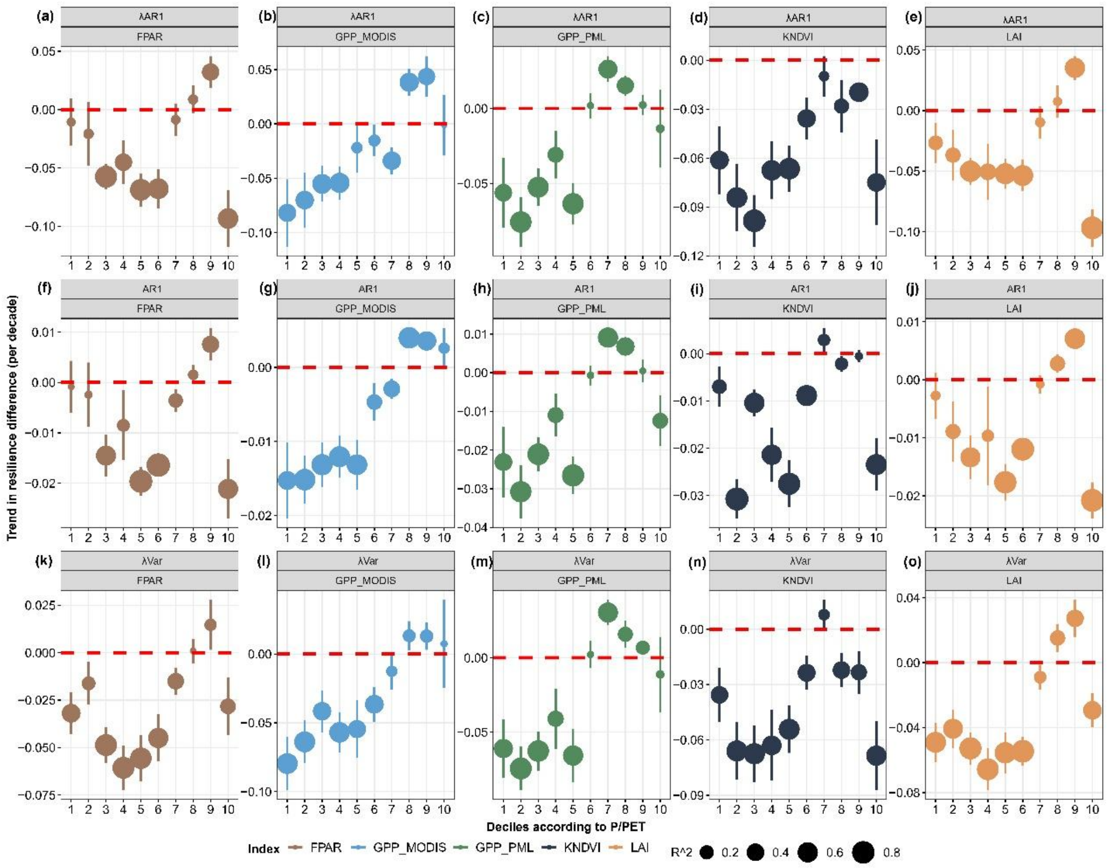

Supplementary Fig. 15. Trends in resilience differences between PF and NF across P/PET gradients (2003–2013). Panels show the decile-based trends (n=822) in resilience differences per decade estimated by (a–e) λAR1, (f–j) AR1, and (k–o) λVar, derived from five vegetation indices: FPAR, GPP_MODIS, GPP_PML, kNDVI, and LAI. The *x*-axis represents deciles of P/PET (aridity index), while the *y*-axis shows the decadal trend in the resilience differences (PF – NF). Circle sizes denote the coefficient of determination (R^2). The point represents the median value for CSD indicator trend, and the highest and lowest bar represents the 1st and 3rd quarter value. The red dashed line represents zero trend.

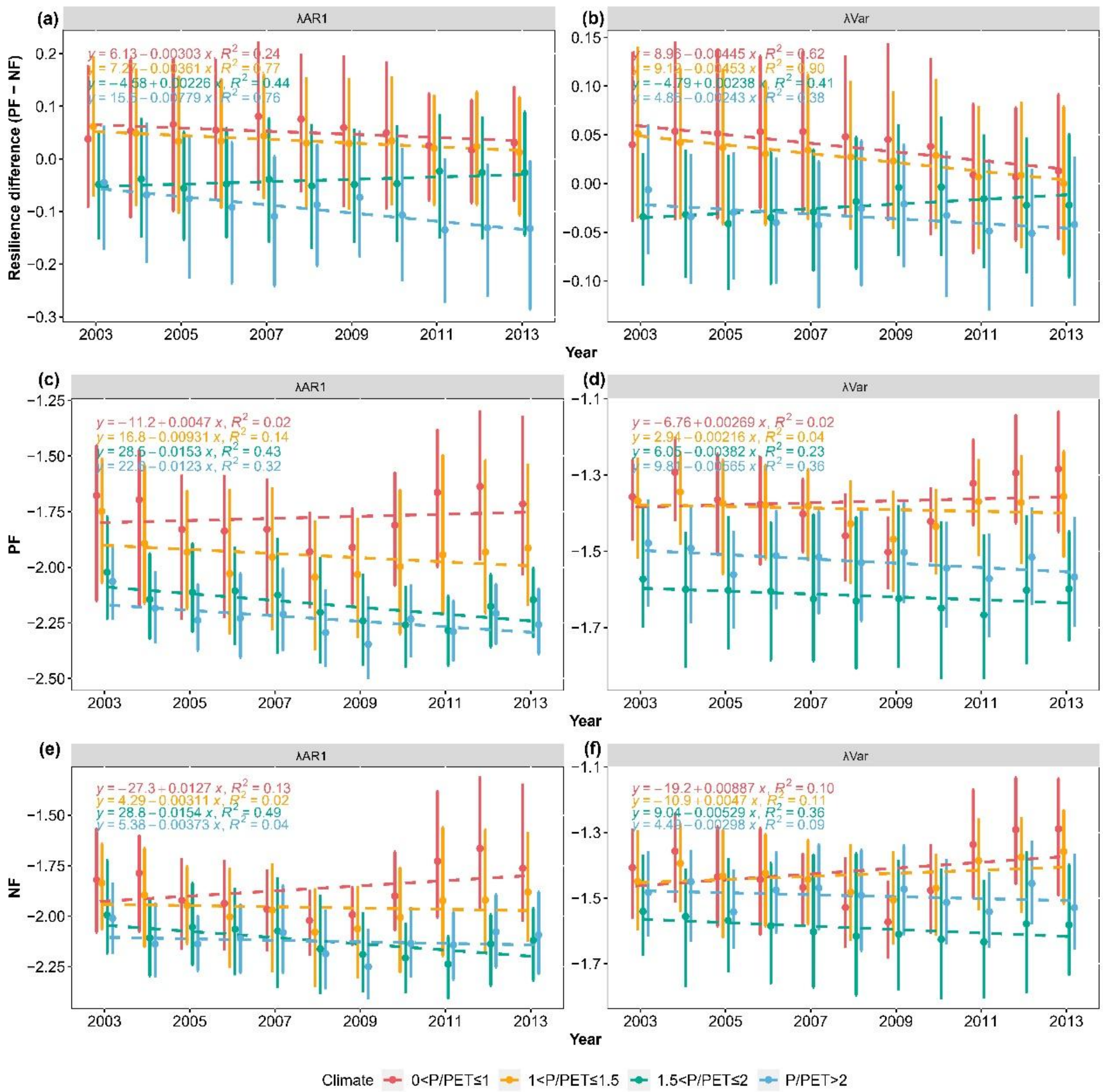

Supplementary Fig. 16. λAR1-LAI and λVar-LAI of PF (c, d) and NF (e, f) and their differences (a, b) across climate zones during 2003–2013, estimated using a 4-year moving window. Colors indicate different aridity zones defined by P/PET: 0–1 (red), 1–1.5 (orange), 1.5–2 (green), and >2 (blue). The point is the median value for CSD indicators, and the highest and lowest bar represents the 1st and 3rd quarter value.

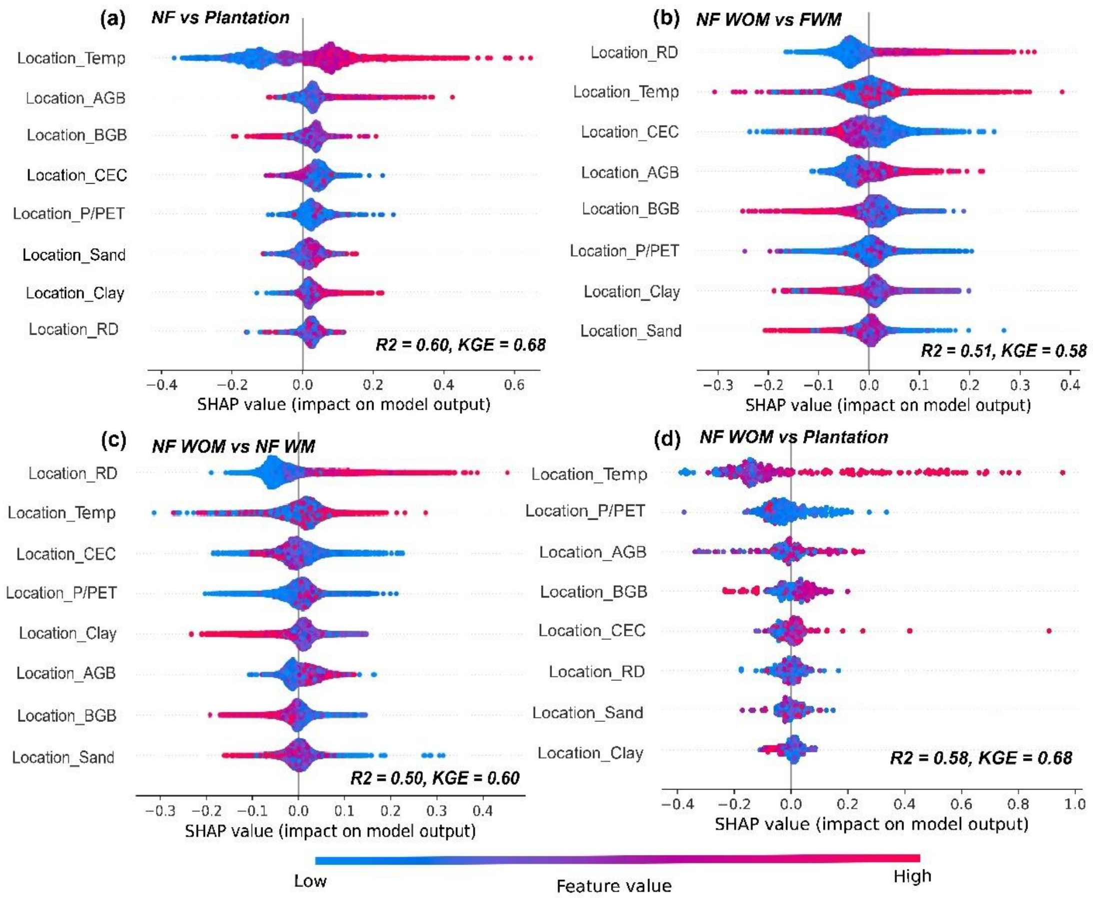

Supplementary Fig. 17. Impact of biophysical factors on resilience difference between different forest management types. Similar to Fig. 4 (and Supplementary Fig. 9b, d), but for the resilience differences between different forest management types. The "Location_Factor" indicates the local biophysical contexts of grids (*y*-axis). SHAP summary plots showing the relative importance of environmental and site factors in predicting the resilience differences across forest management types. Each point represents one sample: colors indicate the feature value (red = high, blue = low), while the SHAP value shows the strength and direction of the feature's effect on the model output (positive = increasing, negative = decreasing). For example, red points with positive SHAP values indicate that high values of the predictor have a positive effect on the target variable, while blue points with negative SHAP values suggest that low predictor values contribute negatively. Four comparisons are presented: (a) NF vs. Plantations, (b) unmanaged natural forests (NF WOM) vs. managed forests (F WM), (c) NF WOM vs. managed NF (NF WM), and (d) NF WOM vs. Plantations. The R^2 and KGE in the lower right corner are derived from the 5-fold cross-validation.

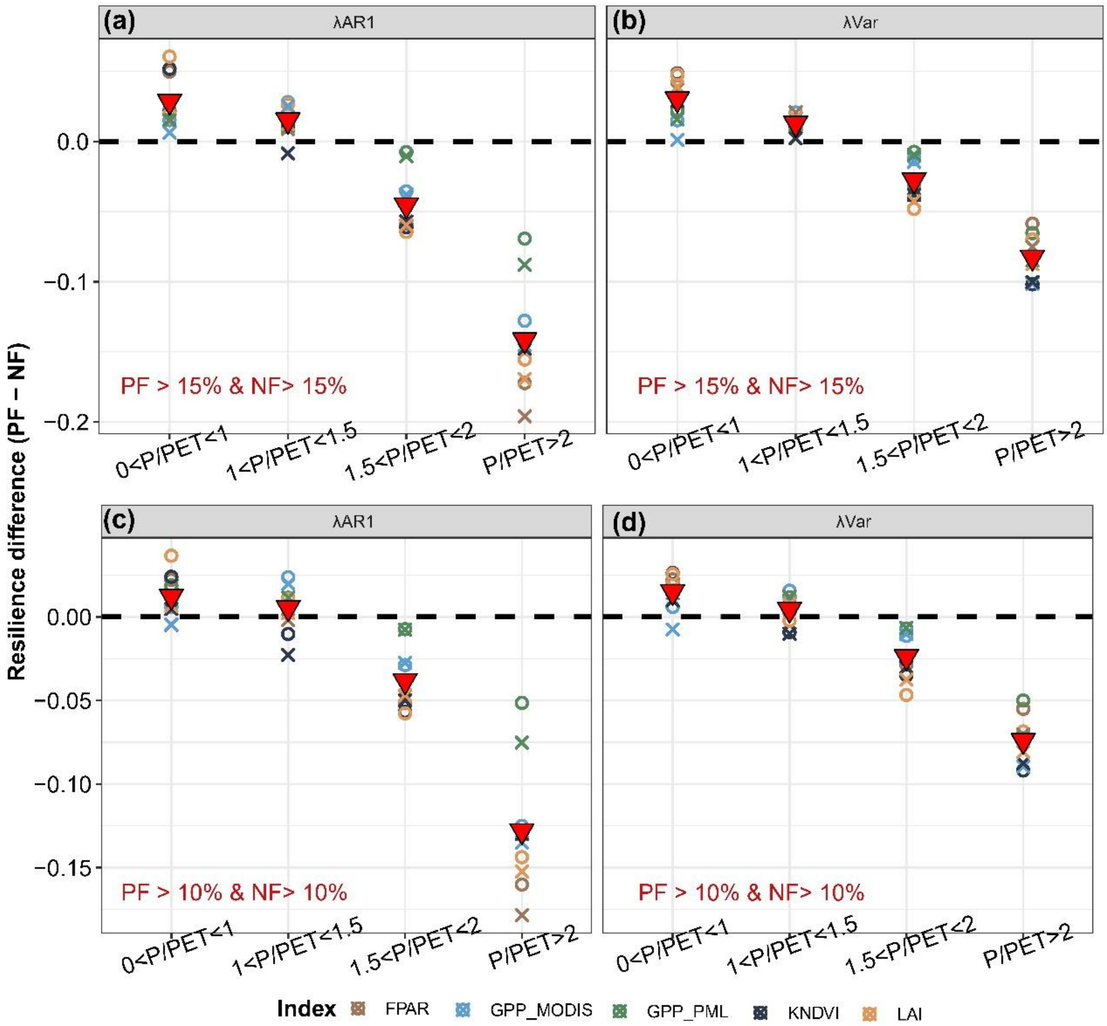

Supplementary Fig. 18. Sensitivity test of resilience differences between PF and NF to the coverage thresholds used in paired-grid selection. Similar to Fig. 3a, b, but for the different thresholds of coverage in paired-grid method. Panels (a, b) show results when both PF and NF coverages exceed 15%, and panels (c, d) when both exceed 10%. The *y*-axis represents the resilience difference (PF – NF), calculated as the mean λAR1 (or λVar) of PF minus that of NF. Results are shown for two resilience indicators, λAR1 (a, c) and λVar (b, d), across P/PET zones. Each marker represents a different vegetation index (FPAR, GPP_MODIS, GPP_PML, kNDVI, LAI).

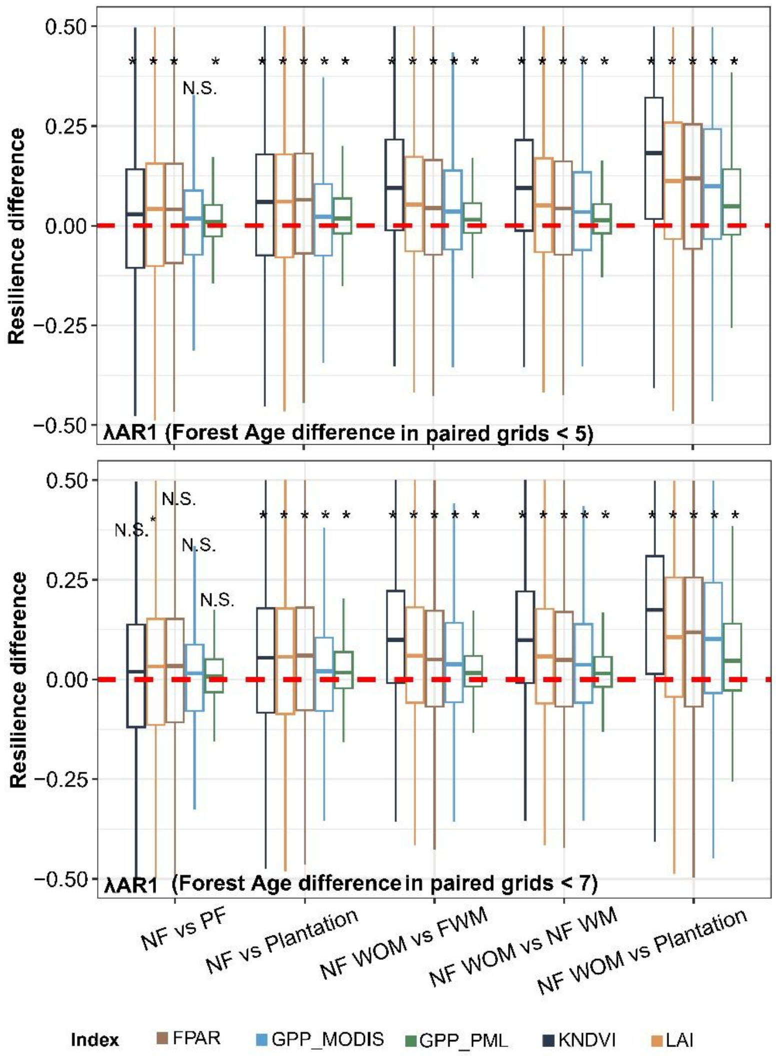

Supplementary Fig. 19. Sensitivity test of resilience differences between forest management types to forest age thresholds in paired-grid selection. Similar to Fig. 2k, but with different thresholds of forests age difference (5 and 7 years) in paired-grid method. Boxplots show resilience differences among forest management types (ΔλAR1, *y*-axis) under alternative thresholds of forest age difference: < 5 years (top) and < 7 years (bottom), compared with the 10-year threshold used in Fig. 2. Results are presented for five vegetation indices (FPAR, GPP_MODIS, GPP_PML, kNDVI, and LAI). Statistical significance was assessed using a two-sided Wilcoxon test to examine whether the resilience difference significantly differs from zero. Asterisks (*) denote significant differences ($p < 0.05$), while N.S. indicates non-significance.

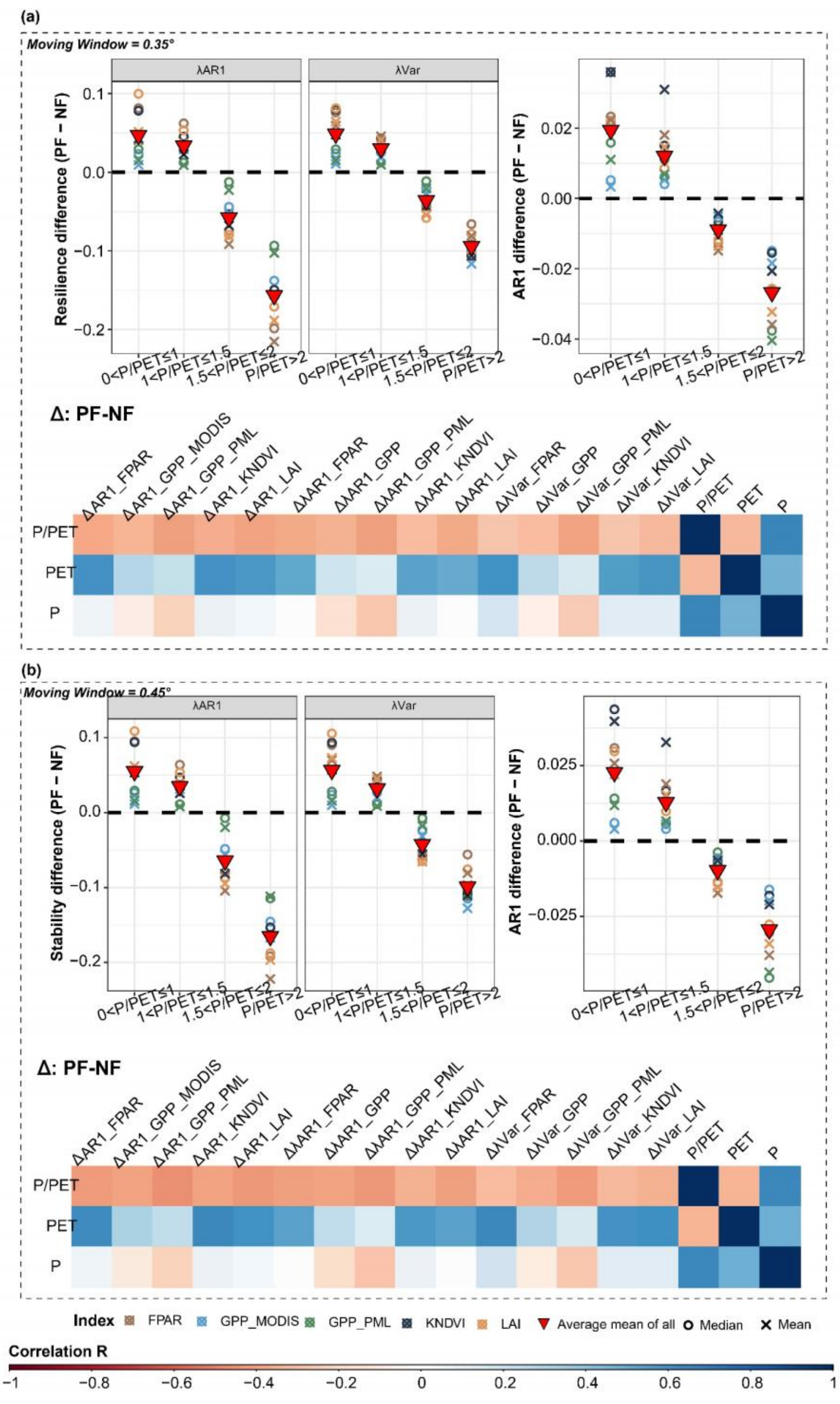

Supplementary Fig. 20. Sensitivity analysis of resilience difference estimation using different moving window sizes. Results are shown for (a) 0.35° × 0.35° and (b) 0.45° × 0.45° window sizes, comparable to those in Fig. 3. Upper panels display resilience differences (PF – NF) across P/PET zones for AR1, λAR1, and λVar derived from multiple vegetation indices, while lower heatmaps show correlations between resilience metrics and climate variables (P/PET, PET, Pre). A cross marks the mean of each vegetation index, a circle denotes the median, and a red inverted triangle indicates the average of the mean and median values.

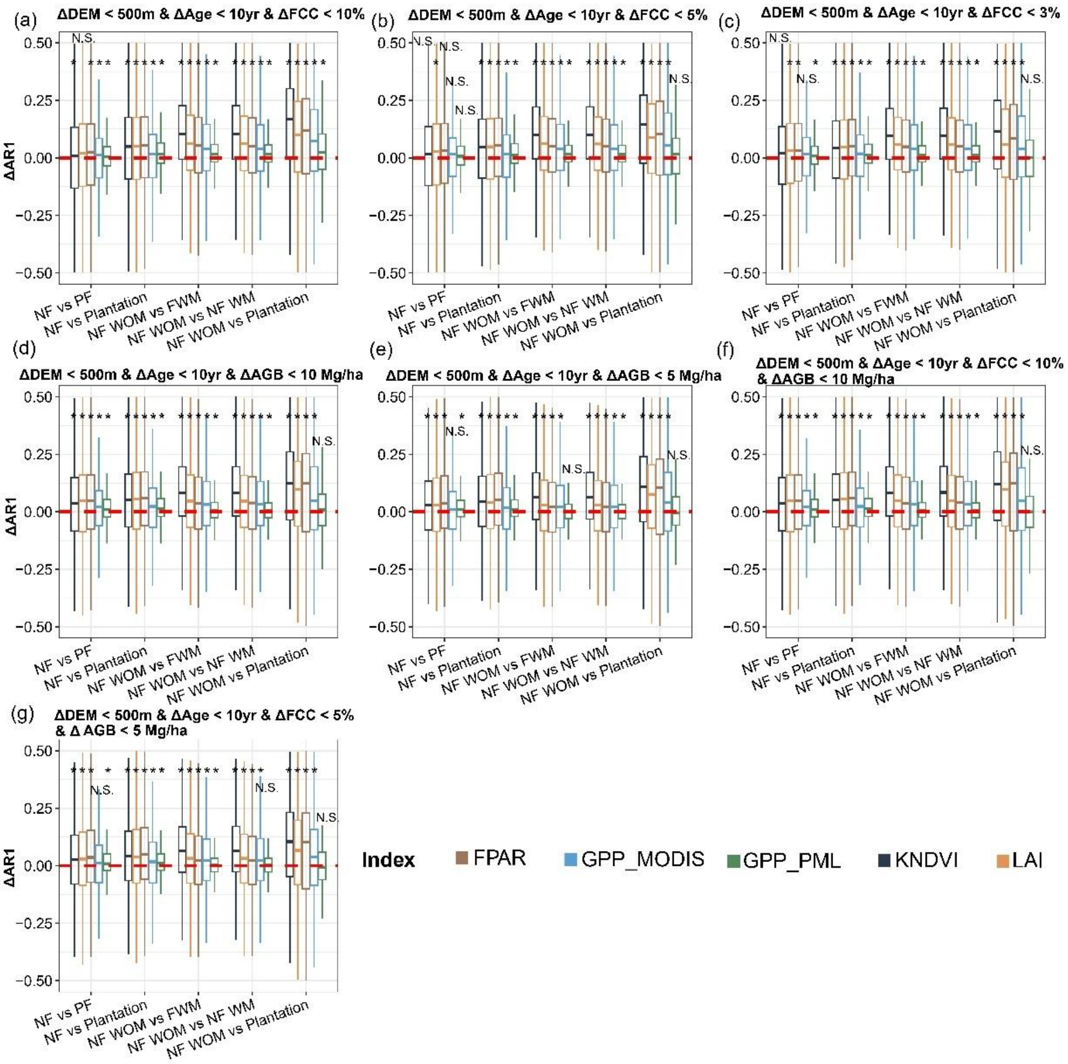

Supplementary Fig. 21. Sensitivity test of different filtering thresholds in paired grid method. The *y*-axis represents the difference in resilience (ΔAR1) between two forest management types (e.g., NF vs PF), where a positive ΔAR1 indicates higher resilience (i.e., lower AR1) in the first forest type (NF). Asterisks denote statistical significance of ΔAR1 differences between paired management types (**p* < 0.05; N.S., not significant), assessed using the two-sided Wilcoxon test. Each boxplot summarizes ΔAR1 across five vegetation indices (FPAR, GPP_MODIS, GPP_PML, kNDVI, and LAI) based on all paired grids that satisfy the corresponding environmental similarity constraints. Panels (a–g) progressively apply stricter thresholds on the differences in elevation (ΔDEM), forest age (ΔAge), forest cover change (ΔFCC), and aboveground biomass (ΔAGB): (a) ΔDEM < 500 m, ΔAge < 10 yr, ΔFCC < 10%; (b) ΔDEM < 500 m, ΔAge < 10 yr, ΔFCC < 5%; (c) ΔDEM < 500 m, ΔAge < 10 yr, ΔFCC < 3%; (d) ΔDEM < 500 m, ΔAge < 10 yr, ΔAGB < 10 Mg ha^{-1}; (e) ΔDEM < 500 m, ΔAge < 10 yr, ΔAGB < 5 Mg ha^{-1}; (f) ΔDEM < 500 m, ΔAge < 10 yr, ΔFCC < 10% and ΔAGB < 10 Mg ha^{-1}; (g) ΔDEM < 500 m, ΔAge < 10 yr, ΔFCC < 5% and ΔAGB < 5 Mg ha^{-1}. Each group of boxplots compares resilience differences between management types, including NF versus PF, NF versus Plantation, NF WOM versus F WM, NF WOM versus NF WM, and NF WOM versus Plantation.

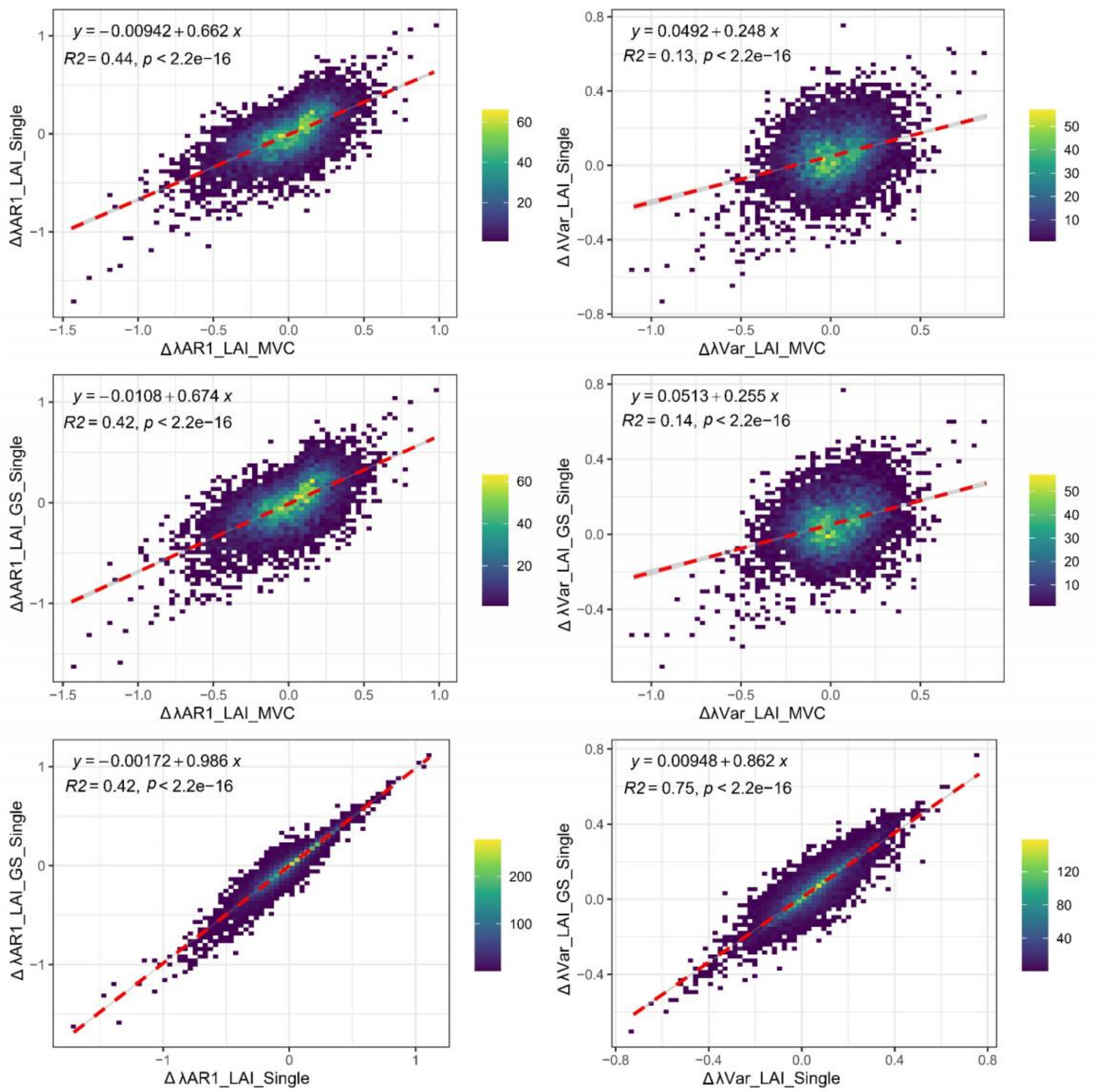

Supplementary Fig. 22. The impacts of time-series pre-processing methods on the resilience difference between PF and NF (e.g., $\Delta\lambda$AR1-LAI$_{(PF,NF)}$). There are three time-series pre-processing methods for estimating resilience by: (1) monthly vegetation index series aggregated via maximum value compositing from MODIS Terra and Aqua LAI datasets (i.e., ΔλAR1_LAI_MVC); (2) the MODIS Terra LAI datasets with its original temporal resolution (no temporal aggregation; i.e., ΔλAR1_LAI_Single); and (3) the Terra time series restricted to the growing season at its original 8-day resolution (i.e., ΔλAR1_LAI_GS_Single). Each scatterplot includes a fitted linear regression (red dashed line) with the regression equation, coefficient of determination (R^2), and significance level (p) shown in the panel. The color bar represents the density of spatial samples, with darker colors indicating lower sample density and brighter colors representing higher density (i.e., more grid cells per bin). The strong linear relationships indicate that the choice of pre-processing method has only minor effects on resilience estimates.

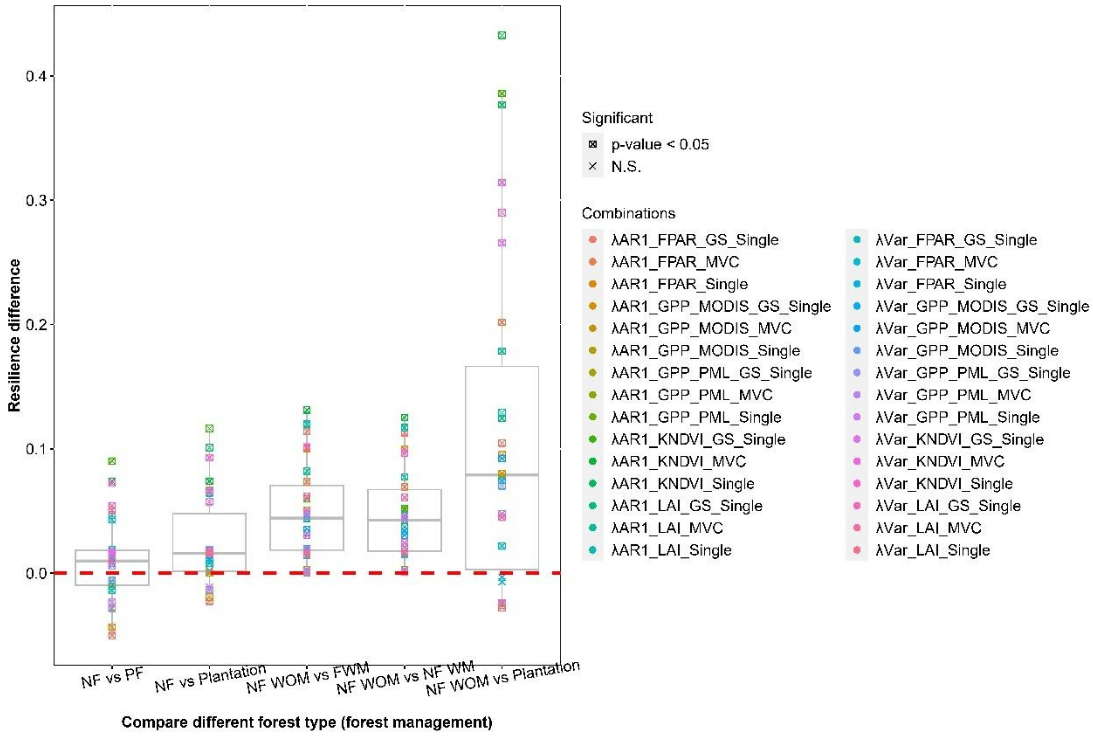

Supplementary Fig. 23. Resilience differences between two forest management types estimated using λAR1 and λVar across multiple vegetation indices and time-series pre-processing methods, as described in Supplementary Fig. 22 caption (GS_Single, MVC, Single). There are three time-series pre-processing methods for estimating resilience by: (1) monthly vegetation index series aggregated via maximum value compositing from MODIS Terra and Aqua LAI datasets (i.e., ΔλAR1_LAI_MVC); (2) the MODIS Terra LAI datasets with its original temporal resolution (no temporal aggregation; i.e., ΔλAR1_LAI_Single); and (3) the Terra time series restricted to the growing season at its original 8-day resolution (i.e., ΔλAR1_LAI_GS_Single). Boxplots compare paired forest types (NF vs PF, NF vs Plantation, NF WOM vs F WM, NF WOM vs NF WM, NF WOM vs Plantation). Each point represents median values from a specific vegetation index and processing method (see legend). Cross symbols denote non-significant differences, while squares enclosing crosses indicate significant differences relative to zero (p < 0.05). Red dashed line represents no resilience difference between two forest management types.

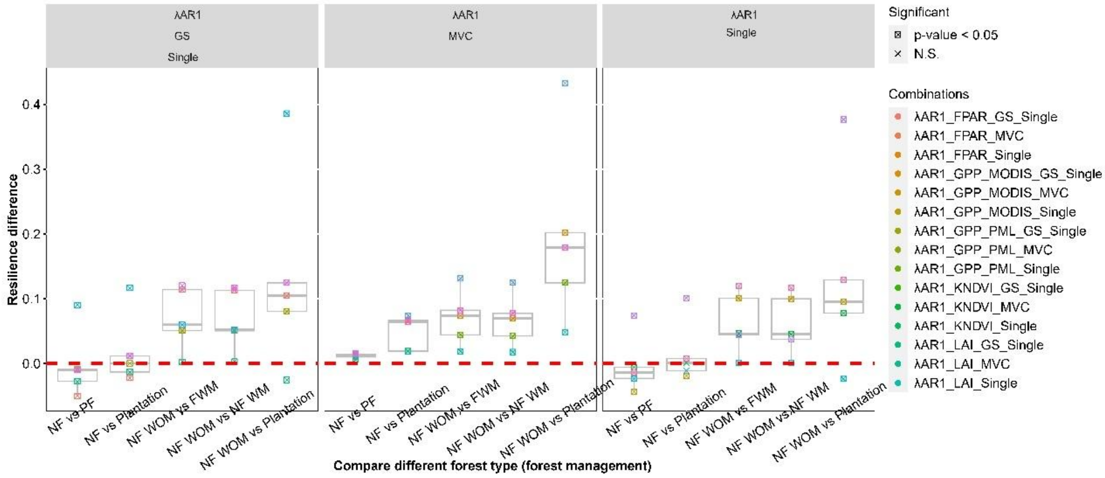

Supplementary Fig. 24. Resilience differences among forest management types estimated using λAR1 across multiple vegetation indices and three time-series pre-processing methods as described in Supplementary Fig. 22 caption (GS_Single, MVC, Single). There are three time-series pre-processing methods for estimating resilience by: (1) monthly vegetation index series aggregated via maximum value compositing from MODIS Terra and Aqua LAI datasets (i.e., ΔλAR1_LAI_MVC); (2) the MODIS Terra LAI datasets with its original temporal resolution (no temporal aggregation; i.e., ΔλAR1_LAI_Single); and (3) the Terra time series restricted to the growing season at its original 8-day resolution (i.e., ΔλAR1_LAI_GS_Single). Boxplots compare paired forest types (NF vs PF, NF vs Plantation, NF WOM vs F WM, NF WOM vs NF WM, NF WOM vs Plantation). Each point represents median values from a specific vegetation index and processing method (see legend). Crosses indicate non-significant differences, while squares enclosing crosses indicate significance relative to zero ($p < 0.05$). Red dashed line represents no resilience difference between two forest management types.

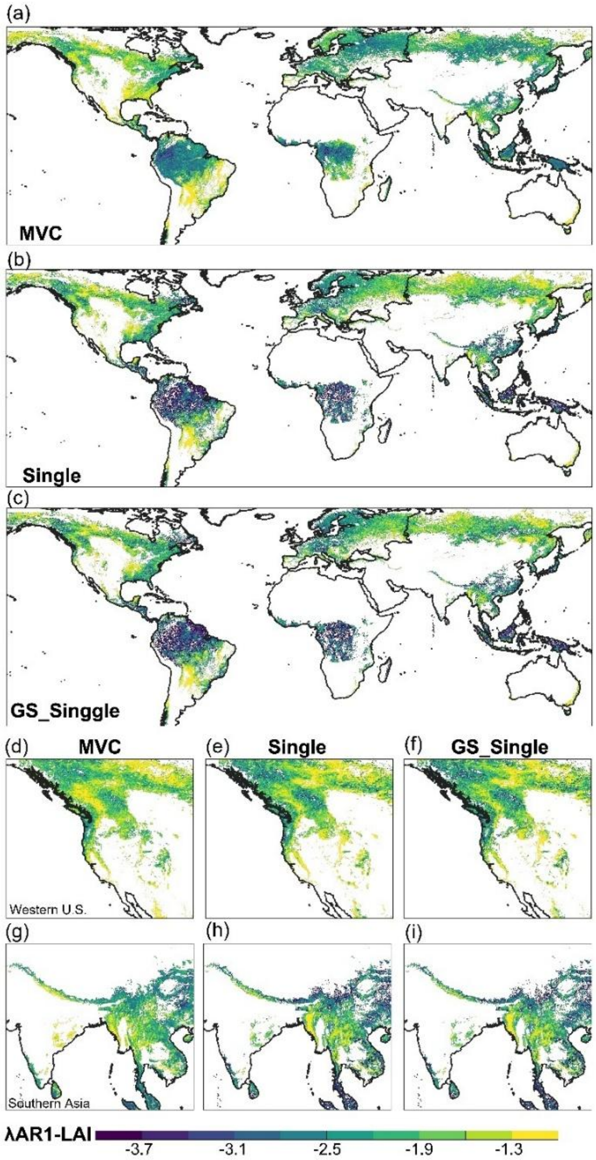

Supplementary Fig. 25. Spatial distribution of long-term λAR1–LAI under different time-series pre-processing methods. Panels (a–c) show global patterns derived from MVC, Single, and GS_Single, respectively. Panels (d–f) and (g–i) show the corresponding results for the western United States and southern Asia. There are three time-series pre-processing methods for estimating resilience by: (1) monthly vegetation index series aggregated via maximum value compositing from MODIS Terra and Aqua LAI datasets (i.e., ΔλAR1_LAI_MVC); (2) the MODIS Terra LAI datasets with its original temporal resolution (no temporal aggregation; i.e., ΔλAR1_LAI_Single); and (3) the Terra time series restricted to the growing season at its original 8-day resolution (i.e., ΔλAR1_LAI_GS_Single).

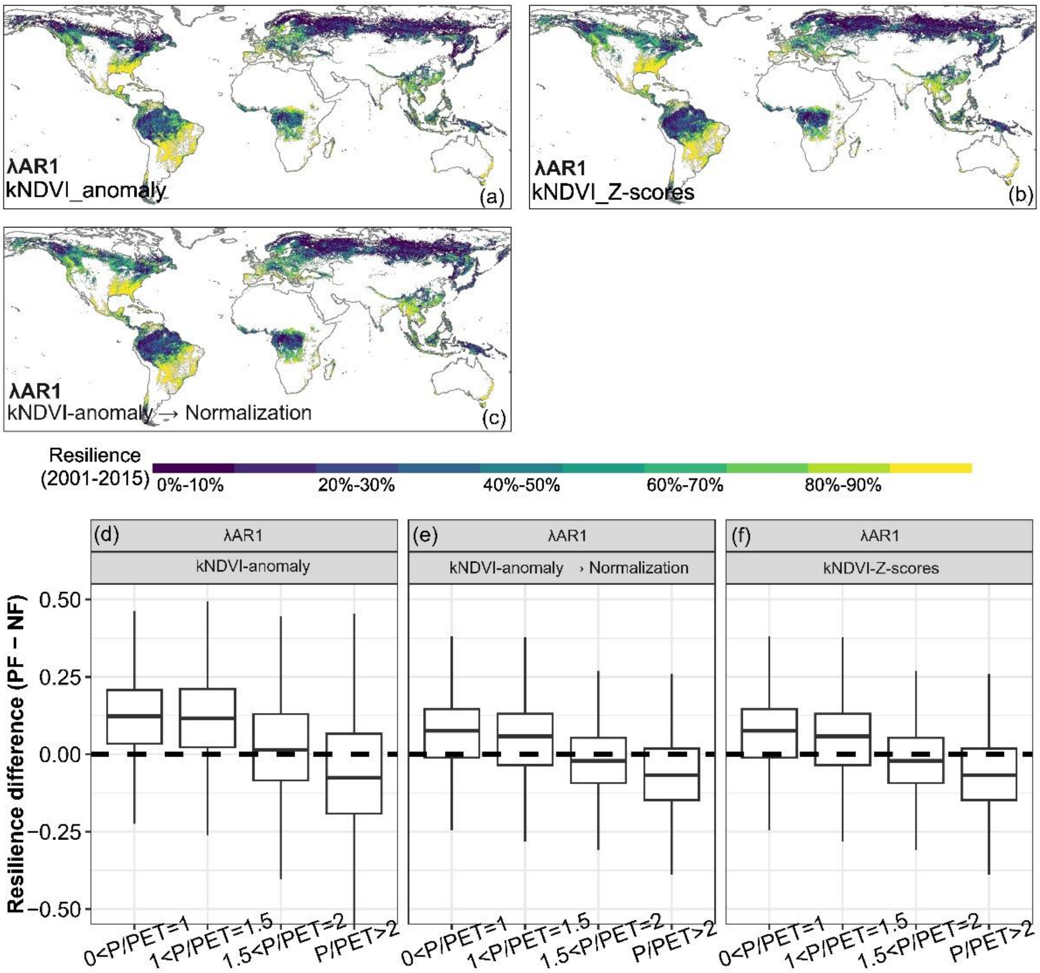

Supplementary Fig. 26. Effect of normalization and standardization methods on resilience estimation. (a–c) Spatial distribution of λAR1 derived from kNDVI anomalies (a), kNDVI Z-scores (b), and normalized kNDVI anomalies (c) for 2001–2015. (d–f) Resilience differences between PF and NF, expressed as ΔλAR1-kNDVI $_{(PF\ -\ NF)}$, estimated with kNDVI anomalies, normalized anomalies, and *Z*-scores under different P/PET gradients.

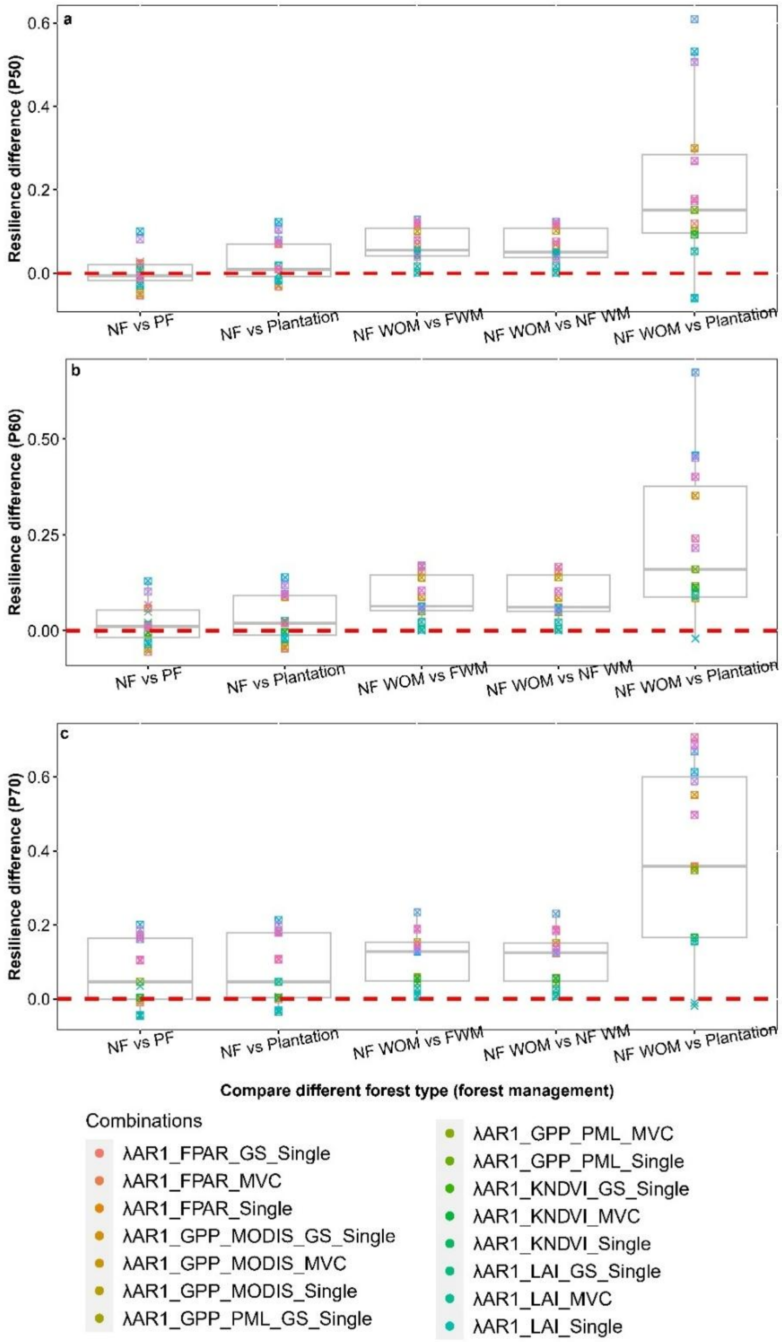

Supplementary Fig. 27. Sensitivity of resilience differences to forest-type classification confidence thresholds. Similar to Fig. S24, but excluding low-confidence forest management classifications based on probability thresholds. Panels (a–c) show resilience differences (ΔλAR1) among forest management types under three classification confidence thresholds: (a) P50, (b) P60, and (c) P70, where only pixels with forest-type classification probabilities above 50%, 60%, and 70% are retained, respectively. The *y*-axis represents the resilience difference (e.g., $\Delta\lambda AR1_{(PF,\ NF)}$), calculated as the λAR1 of PF minus that of NF. Boxplots summarize the distribution of resilience differences across multiple vegetation index combinations, and the red dashed line denotes zero difference.

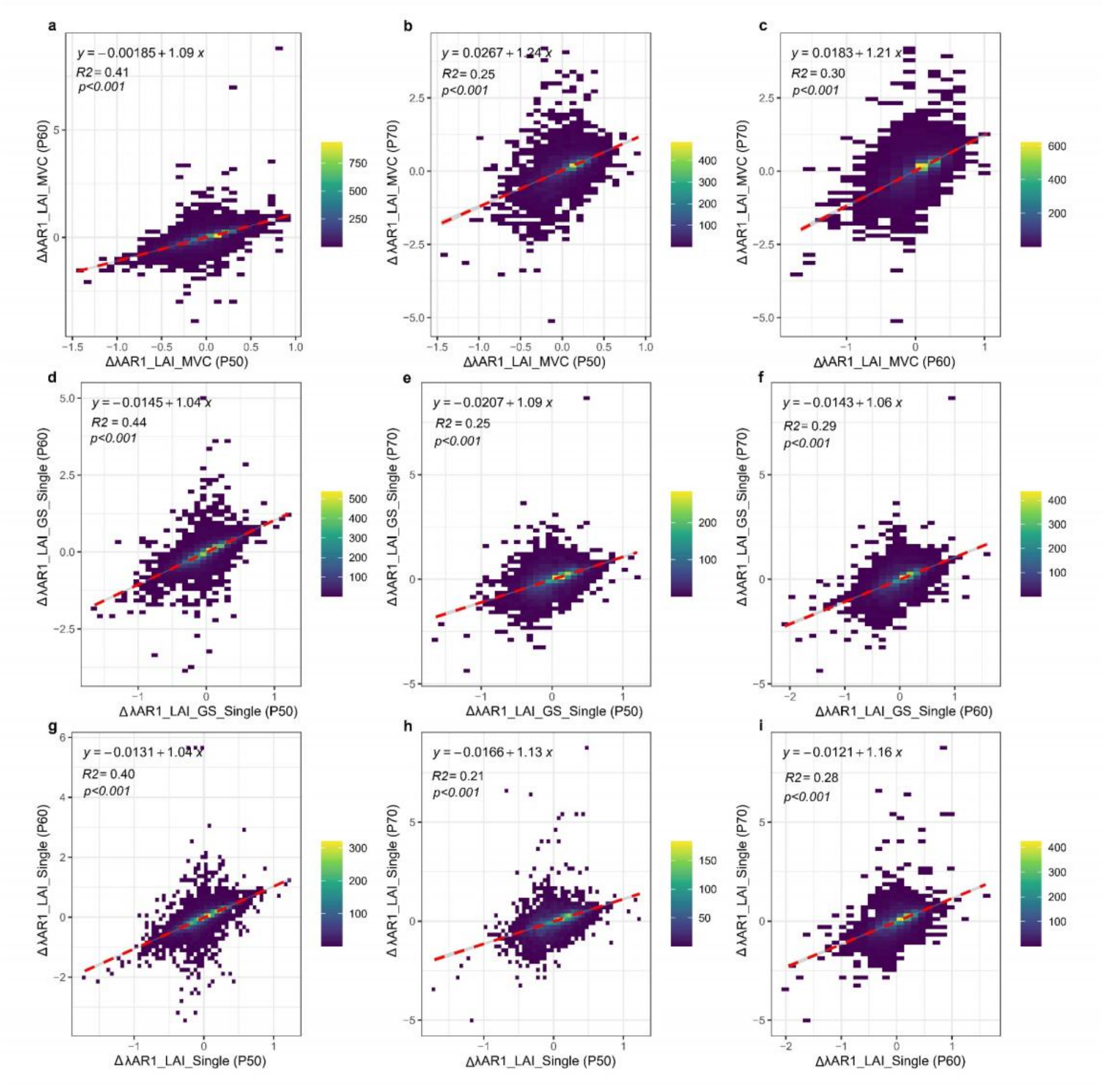

Supplementary Fig. 28. Sensitivity of resilience differences to forest management classification confidence thresholds. Similar to Supplementary Fig. 22, but excluding low-confidence forest management classifications using probability maps. Resilience differences between planted and natural forests (ΔλAR1–LAI, PF – NF) were recalculated under three time-series preprocessing methods: (a–c) monthly maximum value composites (MVC), (d–f) Terra time series restricted to the growing season (GS_Single), and (g–i) Terra time series with the original 8-day temporal resolution (Single). Each row compares results across probability thresholds P50, P60, and P70, where pixels with classification probability below 50%, 60%, or 70% are excluded, respectively. Scatter plots show pairwise comparisons across thresholds, with fitted regression lines (red dashed) and annotated slopes/intercepts. The color bar indicates the density of spatial samples (darker = lower density; brighter = higher density).

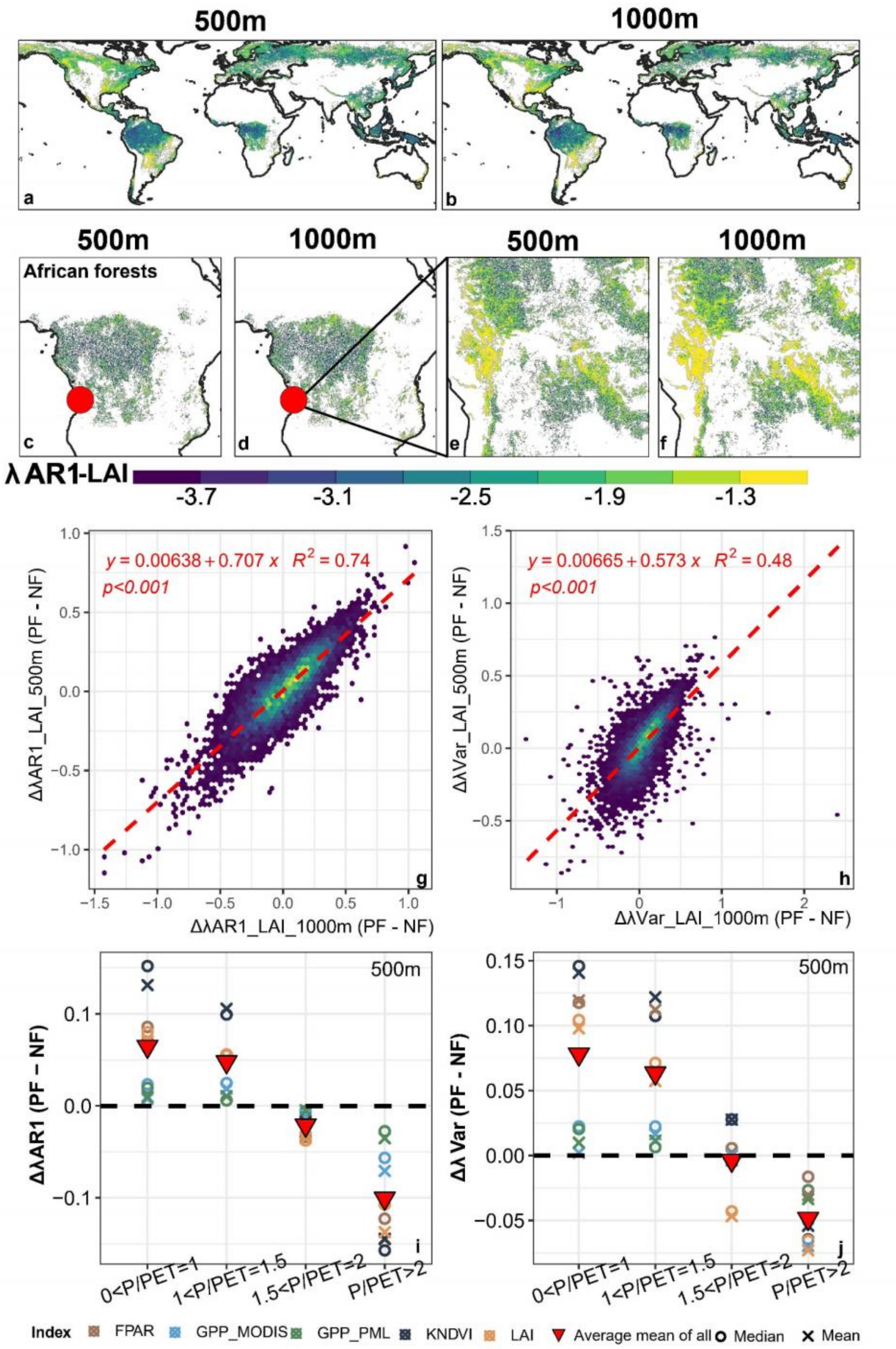

Supplementary Fig. 29. Effect of spatial resolution on forest resilience estimates at 500 m and 1000 m. (a–b) Global maps of λAR1–LAI at 500 m and 1000 m spatial resolutions. (c–f) Comparison of λAR1–LAI patterns in African tropical forests at both resolutions, showing consistent large-scale patterns with localized differences. (g–h) Relationships of resilience differences (ΔλAR1–LAI and ΔλVar–LAI between PF and NF) derived at 500 m versus 1000 m, with corresponding regression lines (red dashed) and coefficients of determination (R^2). (i–j) Mean resilience differences (PF − NF) along precipitation-to-potential-evapotranspiration (P/PET) gradients at 500 m resolution. Each marker represents a vegetation index (FPAR, GPP_MODIS, GPP_PML, kNDVI, and LAI), and red triangles denote the mean across indices.

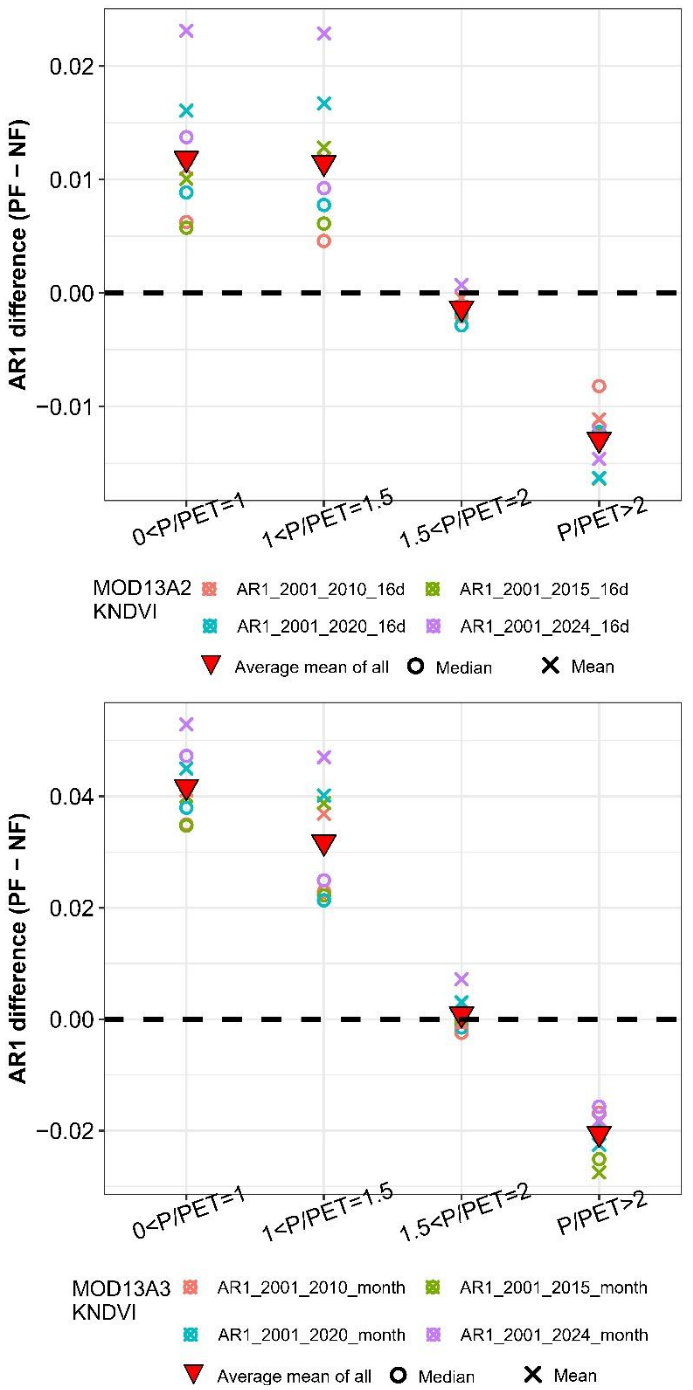

Supplementary Fig. 30. Effect of temporal resolution and time spans on resilience differences between PF and NF. Similar to the Fig. 3c, but by MOD13A2 (16days, 1km) and MOD13A3 datasets (monthly, 1km). Each point represents ΔAR1-kNDVI $_{(PF,\ NF)}$ over different time spans (2001–2010, 2001–2015, 2001–2020, 2001–2024). A cross (×) marks the mean of each vegetation index, a circle (○) denotes the median, and a red inverted triangle (▼) indicates the average of the mean and median values.

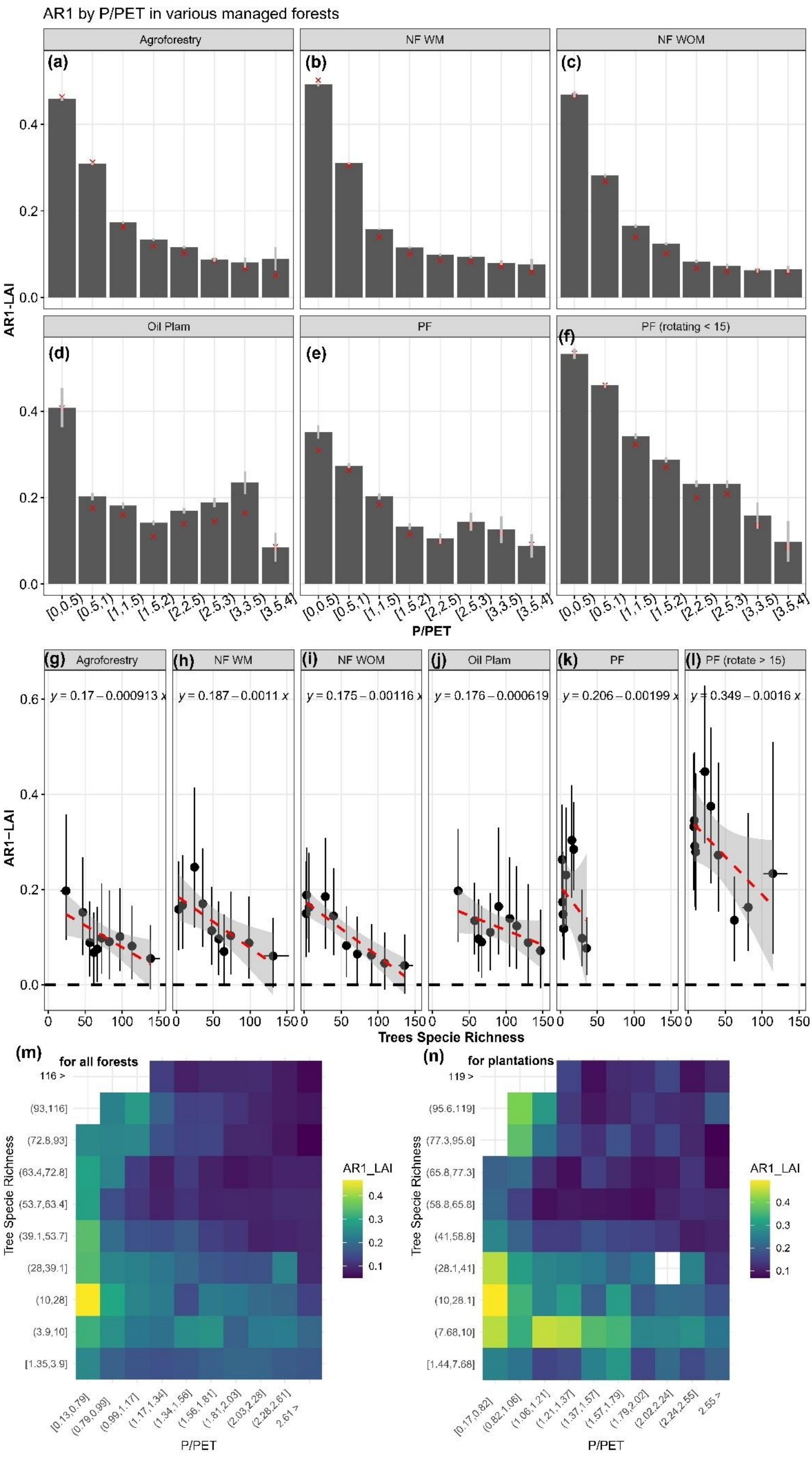
AR1 by P/PET in various managed forests
Agroforestry
NF WM
NF WOM
Oil Plam
PF
PF (rotating < 15)
(a)
(b)
(c)
(d)
(e)
(f)
AR1-LAI
P/PET
[0,0.5)
[0.5,1)
[1,1.5)
[1.5,2)
[2,2.5)
[2.5,3)
[3,3.5)
[3.5,4]
(g) Agroforestry
(h) NF WM
(i) NF WOM
(j) Oil Plam
(k) PF
(l) PF (rotate > 15)
y = 0.17 – 0.000913 x
y = 0.187 – 0.0011 x
y = 0.175 – 0.00116 x
y = 0.176 – 0.000619
y = 0.206 – 0.00199 x
y = 0.349 – 0.0016 x
Trees Specie Richness
(m) for all forests
(n) for plantations
Tree Specie Richness
AR1_LAI
116 >
(93,116]
(72.8,93]
(63.4,72.8]
(53.7,63.4]
(39.1,53.7]
(28,39.1]
(10,28]
(3.9,10]
[1.35,3.9]
[0.13,0.79]
(0.79,0.99]
(0.99,1.17]
(1.17,1.34]
(1.34,1.56]
(1.56,1.81]
(1.81,2.03]
(2.03,2.28]
(2.28,2.61]
2.61 >
119 >
(95.6,119]
(77.3,95.6]
(65.8,77.3]
(58.8,65.8]
(41,58.8]
(28.1,41]
(10,28.1]
(7.68,10]
[1.44,7.68]
[0.17,0.82]
(0.82,1.06]
(1.06,1.21]
(1.21,1.37]
(1.37,1.57]
(1.57,1.79]
(1.79,2.02]
(2.02,2.24]
(2.24,2.55]
2.55 >
P/PET

Supplementary Fig. 31.Relationships among resilience (AR1-LAI), aridity (P/PET), and tree species richness across forest management types, based on the independent crowdsourced dataset. (a–f) AR1-LAI across P/PET bins for agroforestry, NF WM, NF WOM, oil palm, long-rotation PF (>15 years), and short-rotation PF (<15 years). Grey bars show mean values, error bars represent mean ± 2 standard errors (SE), and red crosses denote medians. (g–l) AR1-LAI as a function of tree species richness for the same forest management types, with fitted regression lines (red dashed) and 95% confidence intervals (grey shading). (m–n) Heatmaps showing AR1-LAI as a joint function of tree species richness and P/PET: (m) all forests and (n) Plantations. Grid without color indicates bins with fewer than 50 valid observations.

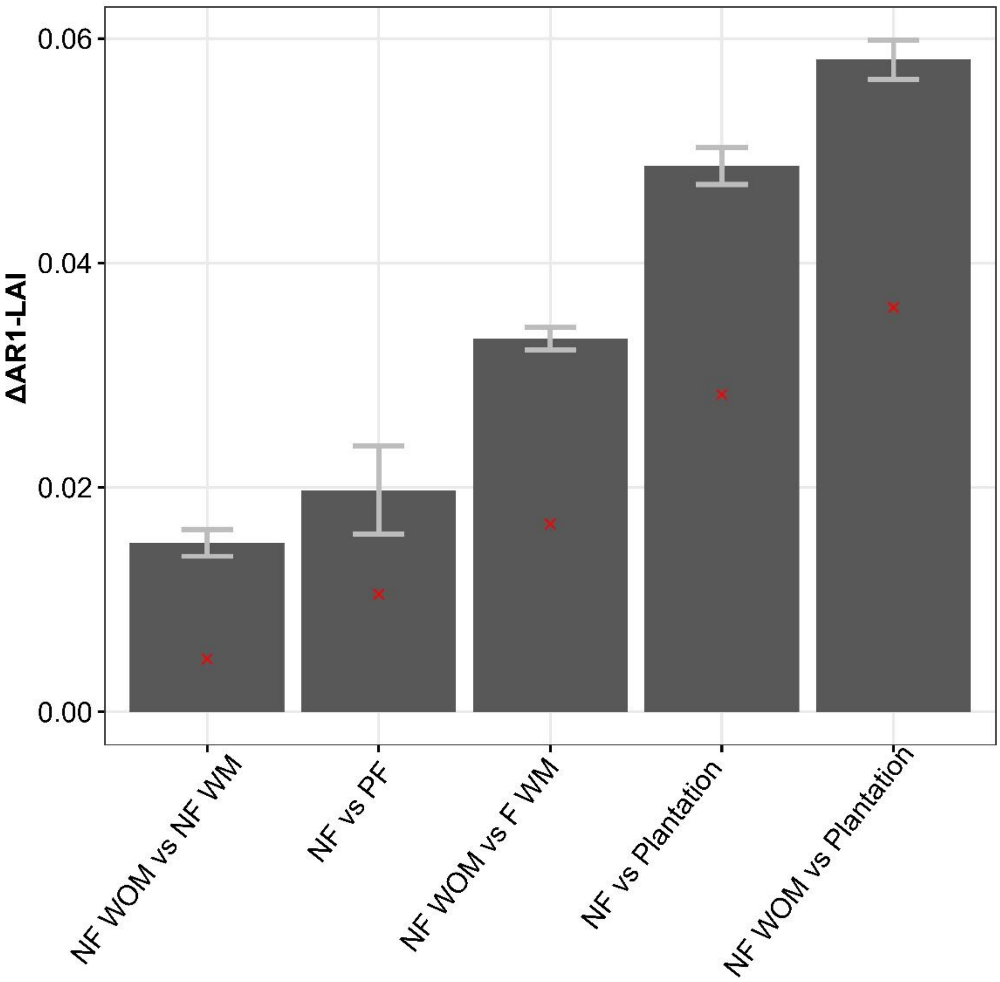

Supplementary Fig. 32. Resilience differences (ΔAR1-LAI) among forest management types based on the independent crowdsourced dataset. Comparisons are performed using a nearest-neighbor matching method (see Supplementary Note 3 for details). Bars represent mean differences with error bars showing mean ± 2*SE, and red crosses indicate medians.

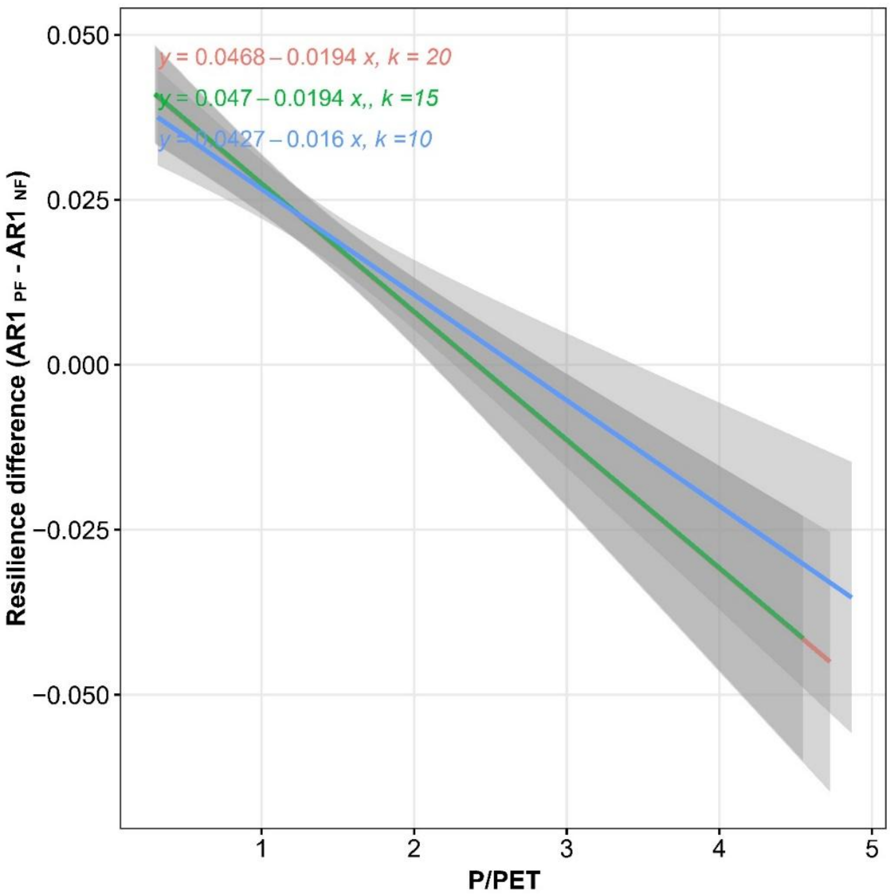

Supplementary Fig. 33. The relationship between the resilience difference (ΔAR1-LAI$_{(PF,NF)}$) and the P/PET by crowdsourced datasets. To account for potential biases in forest type comparison, a nearest-neighbor matching approach is applied, pairing each PF site with environmentally similar NF sites based on geographic proximity and background conditions. To assess the robustness of the results, we tested different matching volumes (k = 10, 15, 20), where *k* denotes the number of matched NF sites assigned to each PF site. Shaded areas indicate the 95% confidence intervals of the fitted regression lines.

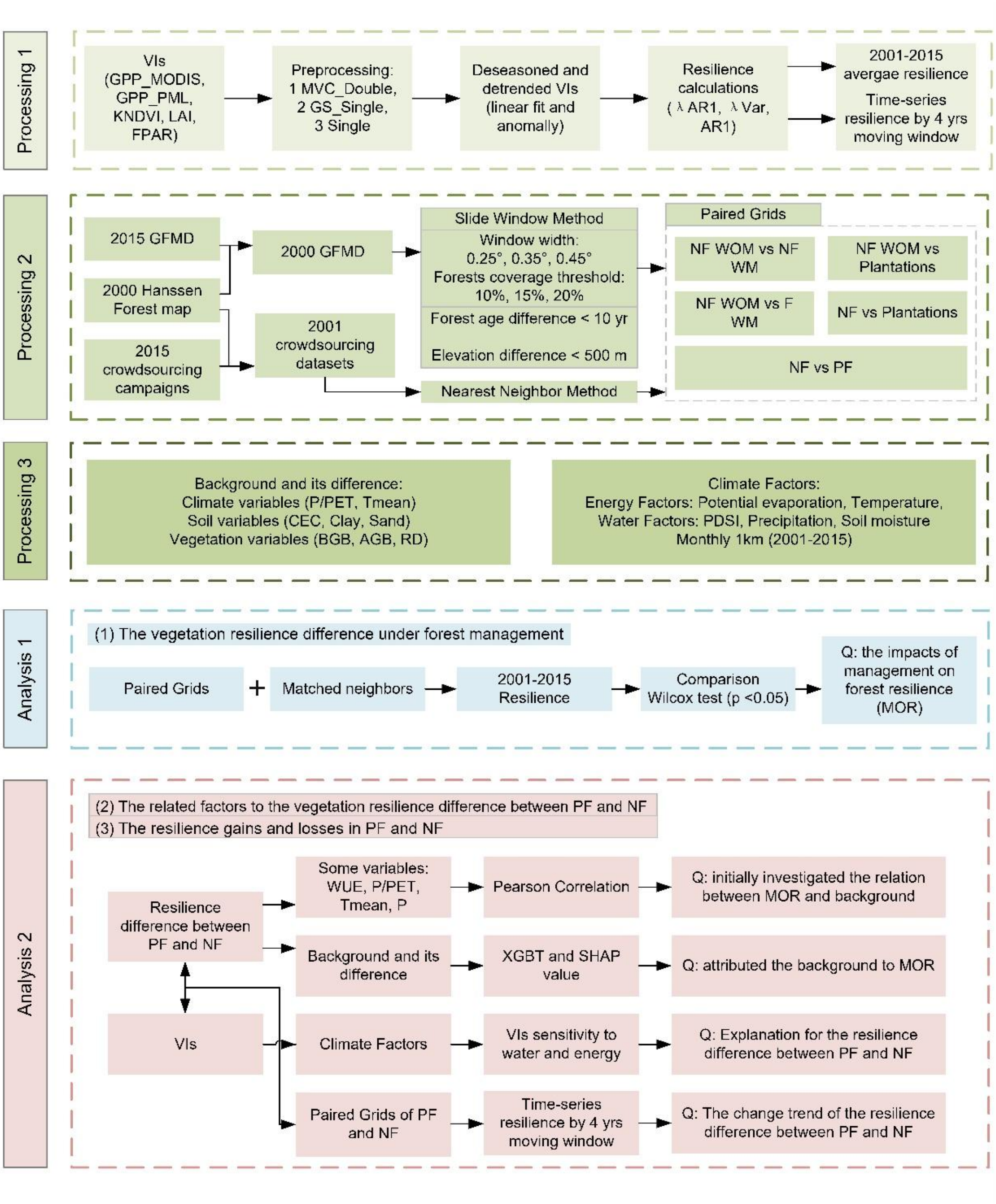

Supplementary Fig. 34. The workflow in this study.

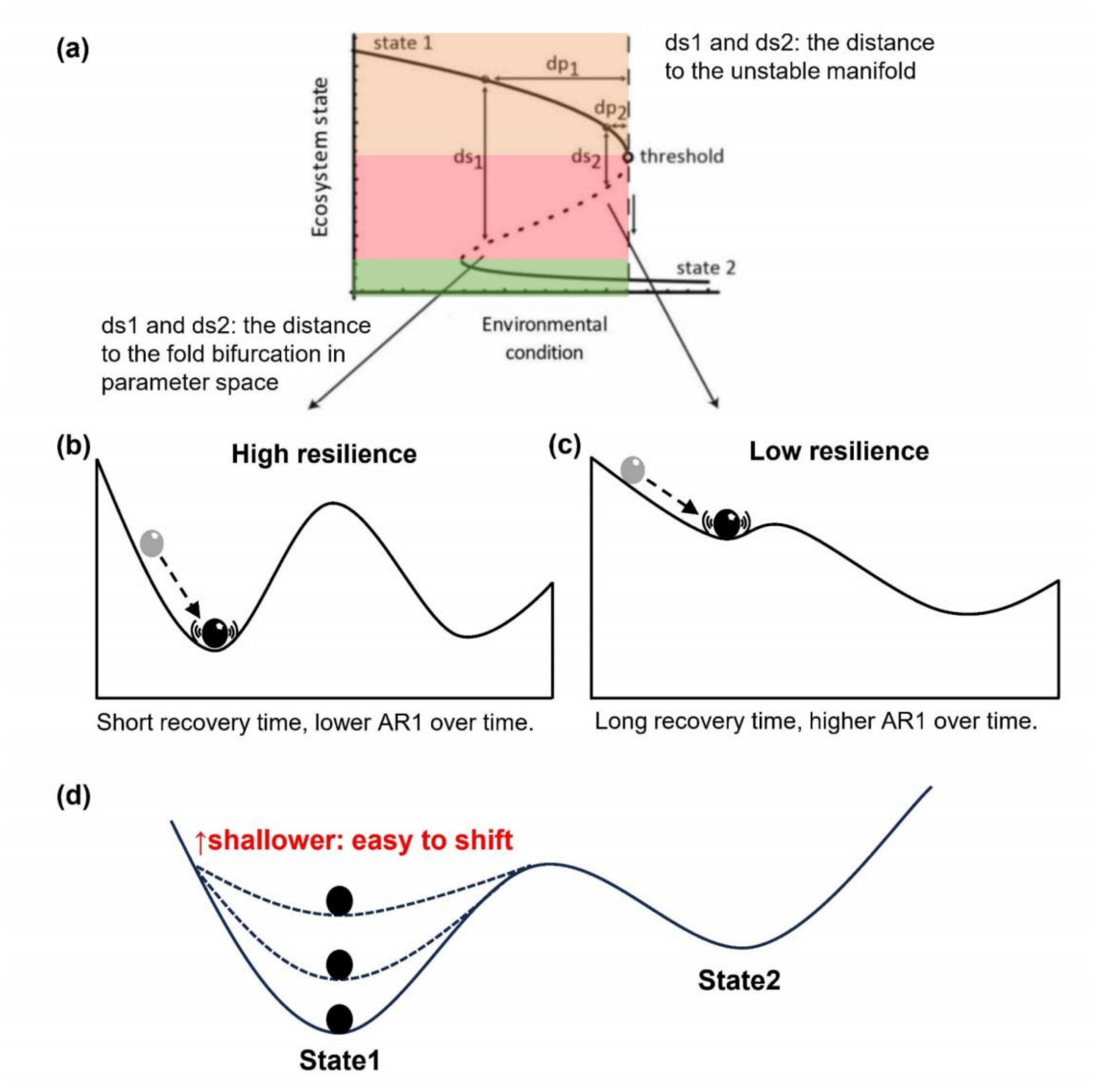

Supplementary Fig. 35. Conceptual illustration of resilience, early warning indicators, and tipping points in ecological systems. (a) Ecosystem state trajectories under changing environmental conditions. This panel depicts how a system can transition from one stable state (state 1) to another (state 2) when a critical environmental threshold (tipping point) is crossed. ds_x is the distance to the unstable manifold (dotted line in (a)), representing the maximum disturbance the system can withstand before shifting states. dp_x is the distance to the fold bifurcation in parameter space (i.e., environmental conditions). (b, c) Basins of attraction illustrating system resilience and corresponding time series properties: (b) High resilience: a deep basin reflects strong capacity to absorb disturbances, characterized by small fluctuations, low autocorrelation (AR1), and low variance. (c) Low resilience: a shallower basin indicates weak capacity to absorb disturbances and maintain equilibrium, with larger fluctuations, higher AR1, and increased variance. (d) Progressive shallowing of the basin of attraction: as the system nears a tipping point, weakening restoring forces reduce its ability to buffer perturbations (i.e., losses of resilience), making a transition to an alternative stable state more likely. These changes in time series properties, particularly increases in AR1 and variance, serve as early warning indicators of impending critical transitions and regime shifts in ecosystems. This figure is modified from refs [11,41,50].

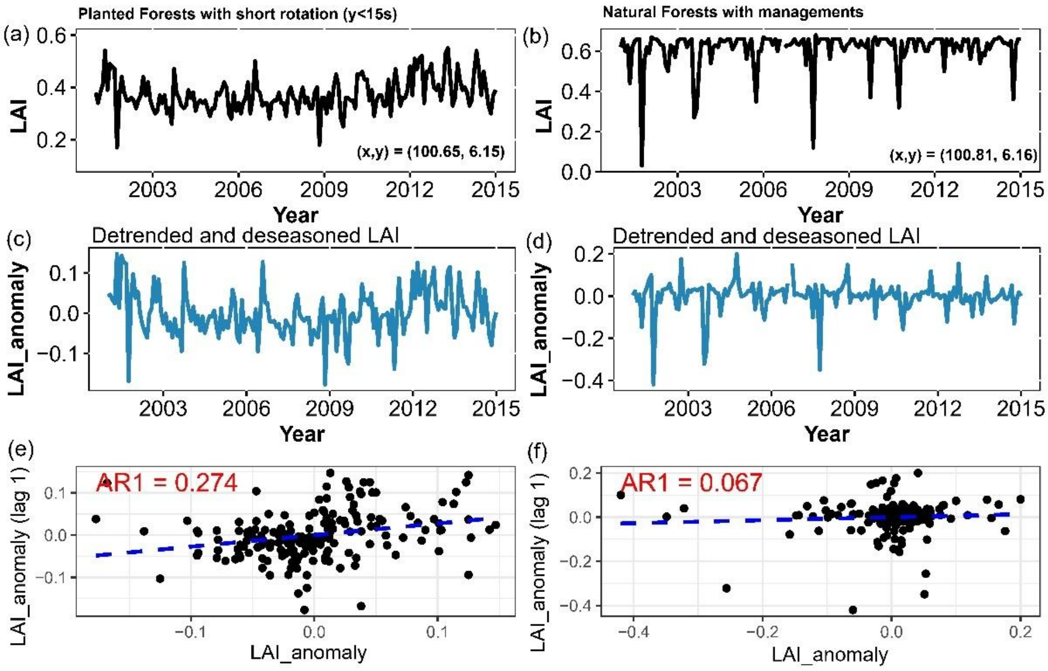

Supplementary Fig. 36. Comparison of LAI anomaly time series and AR1 for nearby different forest management types. (a, b) LAI time series for a planted forest with short-rotation management (100.65°E, 6.15°N) and a nearby natural forest with management (100.81°E, 6.16°N). (c, d) Corresponding LAI anomaly after detrending and deseasonalization. (e, f) Autoregressive lag-1 showing stronger temporal memory in the short-rotation planted forest (AR1-LAI = 0.274) compared to the managed natural forest (AR1-LAI = 0.067)

Supplementary Table 1~Table 3:

Supplementary Table 1. The abbreviation of this study.

Abbreviation	Full Name	Abbreviation	Full Name	Abbreviation	Full Name
NF	Natural Forests	PF	Planted Forests	NF WOM	Natural Forests without Management
NF WM	Natural Forests with Management	F WM	Forests with Management	Plantations	Economic Plantations/Broad definition of PF
GFMD	Global Forest Management Dataset	GHFC	Global Hansen Forest Change	LAI	Leaf Area Index
FPAR	Fraction of Absorbed Photosynthetically Active Radiation	GPP_PML	Gross Primary Productivity (Penman-Monteith-Leuning)	GPP_MODIS	Gross Primary Productivity (MODIS)
kNDVI	Kernel-based Normalized Difference Vegetation Index	NDVI	Normalized Difference Vegetation Index	CSD	Critical Slowing Down
AR1	Auto-regression Lag-1	λAR1	Lambda Auto-regression Lag-1	λVar	Lambda Variance
P/PET	Ratio of Precipitation to Potential Evapotranspiration	PET	Potential Evapotranspiration	Pre	Precipitation
Temp	Temperature	SM	Soil Moisture	PDSI	Palmer Drought Severity Index
RD	Root Depth	CEC	Cation Exchange Capacity	XGBT	Extreme Gradient Boosting Tree
SHAP	Shapley Additive Explanations	MVC	Maximum Value Composite	AGB	Above-Ground Biomass
GHFC	Global Hansen Forest Change	VOD	Vegetation Optical Depth	BGB	Below-Ground Biomass

Supplementary Table 2. Forest management classes and definitions modified by 2015 GFMD[9].

Map ID	Forest management type	Description
11	Naturally regenerating forests without any signs of management, including primary forests	Forests with no or very low human impact: • "not disturbed" – natural forest without detectable evidence of any disturbances within the 100 m pixel and within 500 m in any direction. • "with human impact nearby" – The forest in the classified 100 m pixel is not disturbed, but there are roads or evidence of non-forest management-related human activities (e.g., houses, small agricultural fields) situated nearby (within 500 m in any direction). • "degraded or disturbed" – no human activities in the 100 m pixel or nearby. Forest has been disturbed by natural disturbances, i.e., wildfire, wind throw, flooding, or insect/disease outbreaks.
20	Naturally regenerating forests with signs of forest management, e.g., logging, clear cuts, etc.	Forests with signs of management/cuts in the 100 m pixel or nearby including: • "naturally regenerated forests" – forest is managed with signs of logging (including selected logging) in the 100 m pixel or nearby, but there are no signs of planting. This also includes semi-natural forests – forests without major forest management interventions, which are very similar visually to naturally regenerating forests.
31	Long-rotation planted forests	The forest is managed and there are signs that the forest has been planted in the 100 m pixel (rotating years >15 yr).
32	Short-rotation planted forests	Intensively managed forest plantations for timber (wood plantations, rotating years <15 yr).
40	Oil palm plantations	palms have very distinguishable crown shapes.
53	Agroforestry	Other forest landscapes: • "fruit trees (olives, apples, nuts, cocoa, etc.)". • "Tree shelter belts, small forest patches" – a group of trees on cropland/pastures in lines or patches. • "Agroforestry or sparse trees on agricultural fields" – mixed crops (including trees) or individual trees on cropland or pasture. • "Shifting cultivation" – a form of agriculture, in which an area is cleared of vegetation and cultivated for a few years and then abandoned for a new area until its fertility has been naturally restored. Usually, one can see pieces of land with all the stages of this process. • "trees in urban/built-up areas" – buildings or infrastructure dominant in the 100 m pixel or surroundings.

Supplementary Table 3. The information for the vegetation products used in this study

Index	Datasets	Spatial and temporal resolution	Sources
GPP_PML	PML_V2 0.1.7	8 days/500 m	https://onlinelibrary.wiley.com/doi/10.1002/eco.1974
GPP_MODIS	MOD17A2H.061 (MODIS Terra) MYD17A2H.061 (MODIS Aqua)	8 days/500 m	https://lpdaac.usgs.gov/products/mod17a2hv061 https://lpdaac.usgs.gov/products/myd17a2hv061/
LAI	MYD15A2H.061 (MODIS Terra) MOD15A2H.061 (MODIS Aqua)	8 days/500 m	https://lpdaac.usgs.gov/products/mod15a2hv061/ https://lpdaac.usgs.gov/products/myd15a2hv061/
kNDVI or NDVI	MOD13A2.061 (MODIS Terra) MYD13A2.061 (MODIS Aqua)	16 days/1000 m	https://lpdaac.usgs.gov/products/mod13a3v061/ https://lpdaac.usgs.gov/products/myd13a3v061/
FPAR	MYD15A2H.061 (MODIS Terra) MOD15A2H.061 (MODIS Aqua)	8 days/500 m	https://lpdaac.usgs.gov/products/mod15a2hv061/ https://lpdaac.usgs.gov/products/myd15a2hv061/

Supplementary References:

1. Millar, C. I., Stephenson, N. L. & Stephens, S. L. Climate Change and Forests of the Future: Managing in the Face of Uncertainty. *Ecol. Appl.* **17**, 2145–2151 (2007).
2. Stephenson, N. L. *et al.* Rate of tree carbon accumulation increases continuously with tree size. *Nature* **507**, 90–93 (2014).
3. Luyssaert, S. *et al.* Old-growth forests as global carbon sinks. *Nature* **455**, 213–215 (2008).
4. Cheng, K. *et al.* China's naturally regenerated forests currently have greater aboveground carbon accumulation rates than newly planted forests. *Commun. Earth Environ.* **6**, 1–12 (2025).
5. Yu, Z. *et al.* Natural forests exhibit higher carbon sequestration and lower water consumption than planted forests in China. *Glob. Change Biol.* **25**, 68–77 (2019).
6. Filoso, S., Bezerra, M. O., Weiss, K. C. B. & Palmer, M. A. Impacts of forest restoration on water yield: A systematic review. *PLOS ONE* **12**, e0183210 (2017).
7. Sun, S., Xiang, W., Ouyang, S., Hu, Y. & Peng, C. Balancing Water Yield and Water Use Efficiency Between Planted and Natural Forests: A Global Analysis. *Glob. Change Biol.* **30**, e17561 (2024).
8. Marín-Spiotta, E. & Sharma, S. Carbon storage in successional and plantation forest soils: a tropical analysis. *Glob. Ecol. Biogeogr.* **22**, 105–117 (2013).
9. Liao, C., Luo, Y., Fang, C., Chen, J. & Li, B. The effects of plantation practice on soil properties based on the comparison between natural and planted forests: a meta-analysis. *Glob. Ecol. Biogeogr.* **21**, 318–327 (2012).
10. Cheng, K. *et al.* Carbon storage through China's planted forest expansion. *Nat. Commun.* **15**,

4106 (2024).

11. Forzieri, G., Dakos, V., McDowell, N. G., Ramdane, A. & Cescatti, A. Emerging signals of declining forest resilience under climate change. *Nature* **608**, 534–539 (2022).
12. Lesiv, M. *et al.* Global forest management data for 2015 at a 100 m resolution. *Sci. Data* **9**, 199 (2022).
13. Cheng, K. *et al.* Mapping China's planted forests using high resolution imagery and massive amounts of crowdsourced samples. *ISPRS J. Photogramm. Remote Sens.* **196**, 356–371 (2023).
14. De Frenne, P. *et al.* Forest microclimates and climate change: Importance, drivers and future research agenda. *Glob. Change Biol.* **27**, 2279–2297 (2021).
15. Liu, X. *et al.* Enhancing ecosystem productivity and stability with increasing canopy structural complexity in global forests. *Sci. Adv.* **10**, eadl1947 (2024).
16. Coverdale, T. C. & Davies, A. B. Unravelling the relationship between plant diversity and vegetation structural complexity: A review and theoretical framework. *J. Ecol.* **111**, 1378–1395 (2023).
17. Fan, Y., Miguez-Macho, G., Jobbágy, E. G., Jackson, R. B. & Otero-Casal, C. Hydrologic regulation of plant rooting depth. *Proc. Natl. Acad. Sci.* **114**, 10572–10577 (2017).
18. Getirana, A. *et al.* Deltaic freshwater scarcity driven by unsustainable groundwater-fed irrigation. *Nat. Sustain.* 1–11 (2025) doi:10.1038/s41893-025-01566-0.
19. Buschke, F. & Brownlie, S. Reduced ecological resilience jeopardizes zero loss of biodiversity using the mitigation hierarchy. *Nat. Ecol. Evol.* **4**, 815–819 (2020).

20. Zhang, Y., Keenan, T. F. & Zhou, S. Exacerbated drought impacts on global ecosystems due to structural overshoot. *Nat. Ecol. Evol.* **5**, 1490–1498 (2021).

21. Körner, C., Möhl, P. & Hiltbrunner, E. Four ways to define the growing season. *Ecol. Lett.* **26**, 1277–1292 (2023).

22. Smith, T. & Boers, N. Reliability of vegetation resilience estimates depends on biomass density. *Nat. Ecol. Evol.* **7**, 1799–1808 (2023).

23. Smith, T. & Boers, N. Reliability of vegetation resilience estimates depends on biomass density. *Nat. Ecol. Evol.* **7**, 1799–1808 (2023).

24. McRoberts, R. E. Estimating forest attribute parameters for small areas using nearest neighbors techniques. *For. Ecol. Manag.* **272**, 3–12 (2012).

25. Guo, Q. *et al.* An integrated UAV-borne lidar system for 3D habitat mapping in three forest ecosystems across China. *Int. J. Remote Sens.* **38**, 2954–2972 (2017).

26. Smith, T. & Boers, N. Global vegetation resilience linked to water availability and variability. *Nat. Commun.* **14**, 498 (2023).

27. Devroye, L. & Wagner, T. J. 8 Nearest neighbor methods in discrimination. in *Handbook of Statistics* vol. 2 193–197 (Elsevier, 1982).

28. Liang, J. *et al.* Co-limitation towards lower latitudes shapes global forest diversity gradients. *Nat. Ecol. Evol.* **6**, 1423–1437 (2022).

29. Cazzolla Gatti, R. *et al.* The number of tree species on Earth. *Proc. Natl. Acad. Sci.* **119**, e2115329119 (2022).

30. Dakos, V. *et al.* Slowing down as an early warning signal for abrupt climate change. *Proc.*

Natl. Acad. Sci. **105**, 14308–14312 (2008).

31. Scheffer, M. *et al.* Early-warning signals for critical transitions. *Nature* **461**, 53–59 (2009).
32. Boulton, C. A., Lenton, T. M. & Boers, N. Pronounced loss of Amazon rainforest resilience since the early 2000s. *Nat. Clim. Change* **12**, 271–278 (2022).
33. Huang, K. *et al.* Tipping point of a conifer forest ecosystem under severe drought. *Environ. Res. Lett.* **10**, 024011 (2015).
34. Flores, B. M. *et al.* Critical transitions in the Amazon forest system. *Nature* **626**, 555–564 (2024).
35. Brice, M.-H. *et al.* Moderate disturbances accelerate forest transition dynamics under climate change in the temperate–boreal ecotone of eastern North America. *Glob. Change Biol.* **26**, 4418–4435 (2020).
36. Sáenz-Romero, C. Arriving at a tipping point for worldwide forest decline due to accelerating climatic change. *For. Chron.* **100**, 5–7 (2024).
37. Hajdu, L. H., Meesters, A. G. C. A., Dolman, A. J. & Friend, A. D. Deforestation Could Push Amazonia Close to a Tipping Point Under Future Climate Change. *Geophys. Res. Lett.* **52**, e2024GL108304 (2025).
38. Lenton, T. M., Livina, V. N., Dakos, V., van Nes, E. H. & Scheffer, M. Early warning of climate tipping points from critical slowing down: comparing methods to improve robustness. *Philos. Trans. R. Soc. Math. Phys. Eng. Sci.* **370**, 1185–1204 (2012).
39. Bathiany, S. *et al.* Ecosystem Resilience Monitoring and Early Warning Using Earth Observation Data: Challenges and Outlook. *Surv. Geophys.* **46**, 265–301 (2025).

40. Smith, T. *et al.* Reliability of resilience estimation based on multi-instrument time series. *Earth Syst. Dyn.* **14**, 173–183 (2023).

41. Scheffer, M., Carpenter, S., Foley, J. A., Folke, C. & Walker, B. Catastrophic shifts in ecosystems. *Nature* **413**, 591–596 (2001).

42. Woods, D. D. Four concepts for resilience and the implications for the future of resilience engineering. *Reliab. Eng. Syst. Saf.* **141**, 5–9 (2015).

43. Grimm, V. & Wissel, C. Babel, or the ecological stability discussions: an inventory and analysis of terminology and a guide for avoiding confusion. *Oecologia* **109**, 323–334 (1997).

44. Van Meerbeek, K., Jucker, T. & Svenning, J.-C. Unifying the concepts of stability and resilience in ecology. *J. Ecol.* **109**, 3114–3132 (2021).

45. Engineering, N. A. of. *Engineering Within Ecological Constraints*. (National Academies Press, 1996).

46. Scheffer, M., Carpenter, S. R., Dakos, V. & Nes, E. H. van. Generic Indicators of Ecological Resilience: Inferring the Chance of a Critical Transition. *Annu. Rev. Ecol. Evol. Syst.* **46**, 145–167 (2015).

47. Dakos V. *et al.* Methods for Detecting Early Warnings of Critical Transitions in Time Series Illustrated Using Simulated Ecological Data. *PLOS ONE* **7**, e41010 (2012).

48. Kéfi, S., Saade, C., Berlow, E. L., Cabral, J. S. & Fronhofer, E. A. Scaling up our understanding of tipping points. *Philos. Trans. R. Soc. B Biol. Sci.* **377**, 20210386 (2022).

49. Li, W. *et al.* Unmanaged naturally regenerating forests approach intact forest canopy structure but are susceptible to climate and human stress. *One Earth* **7**, 1068–1081 (2024).

50. Scheffer, M. *et al.* Anticipating Critical Transitions. *Science* **338**, 344–348 (2012).